Spatiotemporal proteomics uncovers cathepsin-dependent macrophage cell death during Salmonella infection

Selkrig, J.; Li, N.; Hausmann, A.; Mangan, M.S.J.; Zietek, M.; Mateus, A.; ... ; Typas, A.

nature microbiology

ARTICLES

https://doi.org/10.1038/s41564-020-0736-7

Check for updates

Spatiotemporal proteomics uncovers cathepsin-dependent macrophage cell death during *Salmonella* infection

Joel Selkrig[1], Nan Li[1,2,3], Annika Hausmann[4], Matthew S. J. Mangan[5,6], Matylda Zietek[1], André Mateus[1], Jacob Bobonis[1,7], Anna Sueki[1,7], Haruna Imamura[8], Bachir El Debs[1,9], Gianluca Sigismondo[3], Bogdan I. Florea[10], Herman S. Overkleeft[10], Nataša Kopitar-Jerala[11], Boris Turk[11,12], Pedro Beltrao[8], Mikhail M. Savitski[1], Eicke Latz[5,6,13], Wolf-Dietrich Hardt[4], Jeroen Krijgsveld[3,14] ✉ and Athanasios Typas[1] ✉

The interplay between host and pathogen relies heavily on rapid protein synthesis and accurate protein targeting to ensure pathogen destruction. To gain insight into this dynamic interface, we combined Click chemistry with pulsed stable isotope labelling of amino acids in cell culture to quantify the host proteome response during macrophage infection with the intracellular bacterial pathogen *Salmonella enterica* Typhimurium. We monitored newly synthesized proteins across different host cell compartments and infection stages. Within this rich resource, we detected aberrant trafficking of lysosomal proteases to the extracellular space and the nucleus. We verified that active cathepsins re-traffic to the nucleus and that these are linked to cell death. Pharmacological cathepsin inhibition and nuclear targeting of a cellular cathepsin inhibitor (stefin B) suppressed *S. enterica* Typhimurium-induced cell death. We demonstrate that cathepsin activity is required for pyroptotic cell death via the non-canonical inflammasome, and that lipopolysaccharide transfection into the host cytoplasm is sufficient to trigger active cathepsin accumulation in the host nucleus and cathepsin-dependent cell death. Finally, cathepsin inhibition reduced gasdermin D expression, thus revealing an unexpected role for cathepsin activity in non-canonical inflammasome regulation. Overall, our study illustrates how resolution of host proteome dynamics during infection can drive the discovery of biological mechanisms at the host–microbe interface.

A successful intracellular pathogen should avoid detection by host cytoplasmic pattern-recognition receptors, which constantly survey the host cytoplasm for microbial ligands. Following detection, activated cytoplasmic pattern-recognition receptors trigger the assembly of a large cytoplasmic protein signalling complex called the inflammasome, which drives an inflammatory form of cell death termed pyroptosis and the release of pro-inflammatory cytokines. Pyroptosis is driven by either the canonical inflammasome cysteine protease caspase-1 (mouse and human) or the non-canonical caspase-11 (mouse) and caspases-4 and -5 (human)[1]. Canonical inflammasome activation relies on additional cytoplasmic sensors to detect bacterial ligands, whereas caspase-11 is both a sensor and activator of the non-canonical inflammasome. Following sensing of lipopolysaccharide (LPS)[2], caspase-11 cleaves gasdermin D into an active form, which then punctures holes in the plasma membrane, ultimately leading to cell death[3,4].

Remarkably, certain intracellular pathogens have evolved to survive and replicate within the hostile endolysosomal system. For example, *Salmonella enterica* subsp. enterica serovar Typhimurium (*S*Tm) sculpts a specialized endolysosomal compartment called the *Salmonella*-containing vacuole (SCV). The SCV provides a membrane-bound shield that prevents detection of *S*Tm surface-bound LPS by the non-canonical inflammasome. When SCV integrity is compromised, bacterial LPS is released to the host cytoplasm where it triggers robust activation of the non-canonical inflammasome and cell death[5]. Thus, although host–pathogen interplay within the endolysosomal system is critical to the survival of both host and pathogen, the dynamics of this process remain poorly understood.

To shed light onto this complex interface, we leveraged a method recently developed in our laboratory designed to enrich, identify and quantify newly synthesized host secretory proteins in serum-containing media[6]. Here, we extended this approach to include sampling of three host cell compartments from *S*Tm-infected macrophages spanning three distinct stages of the infection cycle. We detected aberrant subcellular distribution of lysosomal proteases and demonstrated their active role during *S*Tm-induced cell death via the non-canonical inflammasome. Combined, our findings exemplify

[1]European Molecular Biology Laboratory, Genome Biology Unit, Heidelberg, Germany. [2]CAS Key Laboratory of Quantitative Engineering Biology, Shenzhen Institute of Synthetic Biology, Shenzhen Institutes of Advanced Technology, Chinese Academy of Sciences, Shenzhen, China. [3]German Cancer Research Center, Heidelberg, Germany. [4]Institute of Microbiology, ETH Zurich, Zurich, Switzerland. [5]Institute of Innate Immunity, University of Bonn, Bonn, Germany. [6]German Centre for Neurodegenerative Diseases, Bonn, Germany. [7]Collaboration for joint PhD degree between EMBL and Heidelberg University, Faculty of Biosciences, Heidelberg, Germany. [8]European Bioinformatics Institute, European Molecular Biology Laboratory, Cambridge, UK. [9]BioMedX Innovation Center, Heidelberg, Germany. [10]Department of Bio-organic Synthesis, Leiden Institute of Chemistry, Leiden University, Leiden, the Netherlands. [11]Department of Biochemistry, Molecular and Structural Biology, Jožef Stefan Institute, Ljubljana, Slovenia. [12]Faculty of Chemistry and Chemical Technology, University of Ljubljana, Ljubljana, Slovenia. [13]Department of Infectious Diseases and Immunology, University of Massachusetts Medical School, Worcester, MA, USA. [14]Heidelberg University, Medical Faculty, Heidelberg, Germany. ✉e-mail: j.krijgsveld@dkfz.de; typas@embl.de

the treasure trove of functional biology that can be uncovered by spatiotemporally resolving a host–pathogen interface.

Results

Dynamic proteome mapping unravels diverse host responses during *S*Tm infection. To model the intracellular *S*Tm infection cycle, we infected mouse-derived macrophages with SPI-1 OFF *S*Tm constitutively expressing mCherry from a plasmid (not affecting the infection progress)[7] (Extended Data Fig. 1a). To determine the subcellular distribution of host proteins throughout an infection cycle, we utilized our recently developed proteomic methodology that allows specific enrichment and quantification of the newly synthesized host proteome (Fig. 1a)[6].

We quantified the newly synthesized host proteome (4,978 proteins) by sampling three distinct subcellular locations from macrophages infected with intracellular *S*Tm at 4, 8 and 20 h post infection (hpi). In total we detected 215 proteins in the secretome (conditioned media), 4,640 in the lysatome (Tx-100-soluble; this contains cytoplasmic and organelle content) and 1,283 in the nucleome (Tx-100-insoluble) (Supplementary Table 1, Fig. 1b and Extended Data Fig. 1b). GO term enrichment analysis for host proteins displaying $>1.5 \pm \log_2$(fold-change) revealed a total of 879 enriched GO terms ($P \leq 0.05$, right-sided hypergeometric test, Bonferroni corrected), with 832 being upregulated and 47 downregulated (Supplementary Table 2). Consistent with the lysatome containing the majority of quantified proteins, 693 enriched GO terms were detected in the lysatome fraction whereas 97 and 87 GO terms were enriched in the nucleome and secretome samples, respectively. We further validated the secretome data using a custom chemokine and cytokine array for seven secreted proteins (Extended Data Fig. 2).

In general terms, dynamic changes occurring at distinct time points of the infection were more frequent in the subcellular compartments, whereas the lysatome was dominated by constant responses occurring from the first time point (4 hpi) and remaining stable across time (Fig. 1b). Such early and stable responses included many GO terms related to infection and adaptation to immune stimulation (Supplementary Discussion). For example, in secretome samples, lysosomal proteins displayed enhanced secretion at 20 hpi (GO:0005764; Fig. 1b and Supplementary Table 2). Similarly to the secretome, lysosomal components (GO:0005764; Fig. 1b), consisting of many lysosomal proteases—for example, cathepsins A (CtsA), B (CtsB), D (CtsD), L (CtsL), S (CtsS) and Z (CtsZ) and legumain (Lgmn)—were more abundant in the nuclear fraction. This nuclear enrichment was specific for cathepsins because other lysosomal lumen proteins, such as aryl-sulfatase and α-glucosidase, were abundant in the lysatome but not detected in the nucleome. Similarly, only a handful of cytosolic proteins showed increased abundance in the nucleome during the late stages of infection, including peroxiredoxins 1, 2 and 4, a ubiquitous family of antioxidant enzymes (Supplementary Table 3).

***S*Tm infection induces distinct host proteome responses compared to LPS.** We anticipated that most of the responses in our experimental design would be attributable to the highly immunogenic LPS present on the *S*Tm cell surface. To test this, we directly compared our lysatome samples from *S*Tm-infected cells with previously published data from RAW264.7 cells stimulated with LPS[8] (Supplementary Table 3). The two time points analysed span two distinct phases of the *S*Tm intracellular life cycle, namely (1) pre-SPI-2-dependent proliferation (3–4 h) and (2) active SPI-2-dependent growth (8 h). Consistent with our expectations, *S*Tm infection and LPS stimulation showed strong positive correlations at both 4 h ($r = 0.65$) and 8 h ($r = 0.635$) (Fig. 2a,b). Thus, much of the proteome response of *S*Tm-infected cells can be explained by innate immune responses to LPS per se. Beyond the overall similarity, we could identify host responses specific to *S*Tm infection by filtering out the LPS response from *S*Tm-infected samples and performing GO term enrichment (Fig. 2a,b, Supplementary Tables 4 and 5 and Supplementary Discussion).

We then compared the secretome of LPS- and *S*Tm-treated cells (Fig. 2c). Similar to the lysatome, *S*Tm infection and LPS stimulation induced broadly similar protein secretion dynamics over time (Fig. 2c) although clear differences were again apparent. The most profound difference was the enhanced secretion of lysosomal hydrolases, including CtsC, CtsL, CtsD, CtsZ, CtsA and Lgmn, during *S*Tm infection (Fig. 2c). Interestingly, *S*Tm was previously shown to enhance the secretion of both β-hexosaminidase and immature CtsD, ultimately depriving lysosomes of hydrolytic enzymes to promote *S*Tm proliferation[9]. Our findings suggest that *S*Tm-induced lysosomal detoxification is broader than previously appreciated.

Lysosomal proteases are enriched in the nuclear fraction during *S*Tm infection. Reminiscent of *S*Tm-induced secretion of lysosomal proteases observed in the secretome, we also detected a strong and significant increase in several lysosomal hydrolases at 20 hpi in the nucleome (Fig. 3a). Because the expression levels of these proteins increased only marginally in the lysatome samples (Fig. 3b,c), their much stronger increase in the nucleus is presumably due to their increased trafficking to this compartment. We excluded the possibility that this may be due to co-fractionation of lysosomal components together with the nucleus in our experiments, as Lamp1 and Lamp2 were detected only in the lysatome (Supplementary Tables 1 and 3). Although some vacuolar membrane proteins were also enriched in the nuclear fraction, this was at a much lower level than

Fig. 1 | Newly synthesized proteome enrichment detects diverse host responses during *S*Tm infection. a, Experimental design of pSILAC-AHA labelling and subcellular fractionation. (i) RAW264.7 cells were infected with *S*Tm 14028s constitutively expressing mCherry (pFCcGi) and grown to stationary phase at MOI = 100:1, followed by centrifugation to facilitate host–pathogen contact. After incubation for 25 min, extracellular *S*Tm were killed by moving cells first to media containing 100 μg ml^{-1} gentamicin for 1 h, and then to media containing 16 μg ml^{-1} gentamicin for the remainder of the experiment. Uninfected samples received a mock inoculum and were otherwise treated identically to infected samples. (ii) 3.5 h before harvest, cells were washed and briefly starved for 30 min to remove residual amino acids, followed by pSILAC-AHA labelling for 3 h. A 3-h pulse window is sufficient to allow protein synthesis and subsequent subcellular trafficking[8]. (iii) Conditioned media were harvested for the secretome samples, whereas cells were washed and partially lysed with a mild detergent (Triton X-100) to extract both the lysatome and nuclear samples. (iv) Samples were mixed at 1:1 ratio (infected:uninfected) and then fractionated by centrifugation to separate the secretome, nucleome and lysatome. (v) Newly synthesized proteins containing AHA were covalently linked to alkyne agarose beads via a Click chemistry reaction, allowing for selective capture of proteins containing incorporated AHA, while serum and other pre-existing background proteins were removed by stringent washing conditions. (vi) After on-bead protease digestion, peptides were quantified by LC–MS/MS. (I) and (H) refer to intermediate and heavy isotopic amino acids, respectively. (P) and (S) denote pellet and supernatant, respectively. Icons distributed under the terms of the Creative Commons Attribution 4.0 International License (http://creativecommons.org/licenses/by/4.0/) were adapted with permission from ref. [32], Springer Nature Limited. **b**, GO term enrichment of differentially regulated host proteins (4, 8 and 20 h). Selected enriched GO terms are depicted; all enriched GO terms can be found in Supplementary Table 2. Node size and colours depict significance, (P ($-\log_{10}$) right-sided hypergeometric test, Bonferroni corrected) and number of proteins (blue shading), respectively. ND, not determined. $n = 2$ biologically independent samples.

their luminal counterparts. This suggested that cathepsin enrichment (luminal proteins) cannot be generally explained by increased levels of lysosomal proteins in the nucleome per se (Fig. 3c). Instead, we hypothesized that newly synthesized lysosomal proteins are trafficked to the nucleus during *S*Tm infection. Although cathepsins have previously been observed in the nucleus[10–13], this has not been

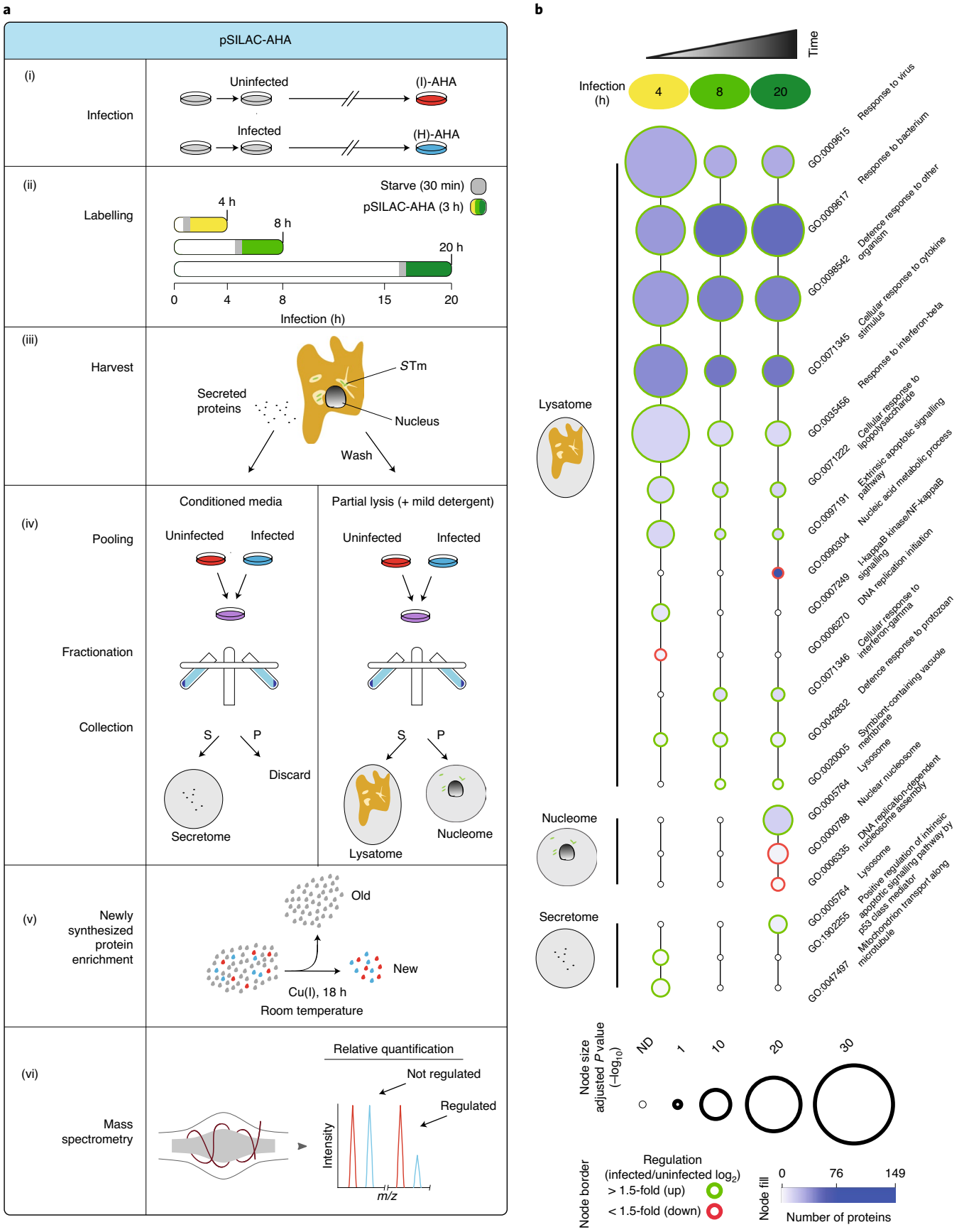

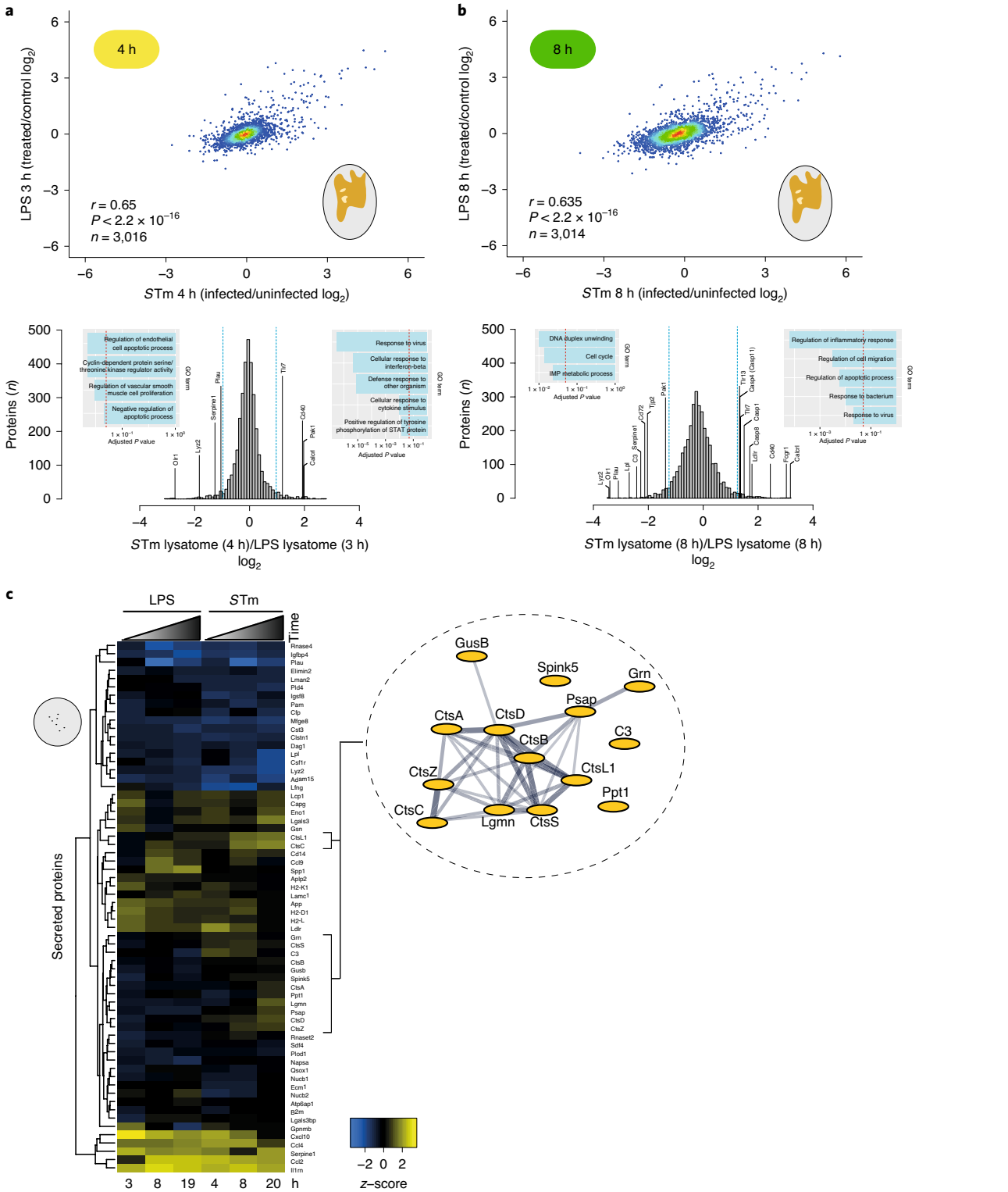

Fig. 2 | *STm* infection induces distinct host proteome responses compared to LPS across time and space. a, Upper: scatter plot of pSILAC-AHA lysatome data previously collected in response to LPS stimulation (LPS from *Escherichia coli* O111:B)[8] versus data collected following *STm* infection from this study (Supplementary Table 3). Note: due to differences in sample collection, LPS samples contain both lysatome and nucleome fractions. Lower: histogram containing protein expression from lysatome of RAW264.7 cells 4 hpi with *STm* after subtracting the $\log_2$ corresponding LPS signal. Dotted blue lines in histogram indicate ±2 s.d. from the mean, and the dotted red line on inset GO term histograms indicates multiple test-adjusted *P* value (Bonferroni corrected) cut-off of 0.05. $n = 2$ biologically independent samples. **b**, Same as **a** but at a later time point: 8 hpi with *STm* or LPS stimulation of RAW264.7. **a**,**b**, Corresponding protein levels can be found in Supplementary Table 4, and GO terms in Supplementary Table 5. $n = 2$ biologically independent samples. **c**, Heat map of secreted proteins from pSILAC-AHA-labelled RAW264.7 cells following either *STm* infection or LPS stimulation, the latter data obtained previously[8]. Note: only rows without missing data points were used for analysis. To the right is a STRING network of vacuolar proteins with increased secretion dynamics specific to *STm* infection. Nodes represent individual proteins, and edges reflect experimentally determined interactions and co-expression weighted data from STRING v.10.5 (ref. [33]).

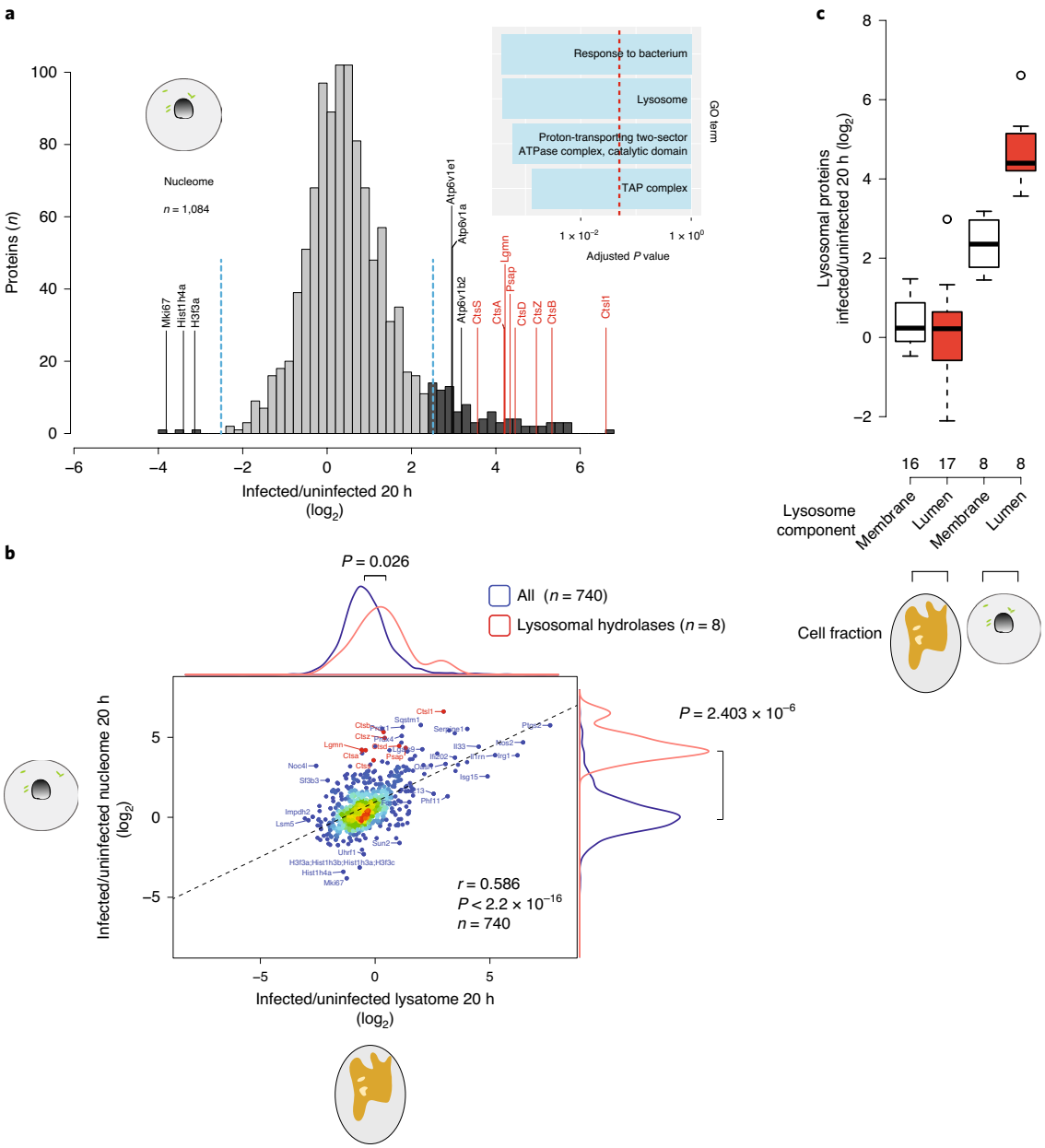

Fig. 3 | Lysosomal proteases are enriched in the nuclear fraction following *STm* infection. a, Histogram of nuclear proteins differentially regulated after 20 h of *STm* infection; lysosomal hydrolases are annotated in red. Blue and red dotted lines, as well as GO cellular component enrichments (inset), as in Fig. 2a. $n = 2$ biologically independent samples. **b**, Scatter plot of lysatome and nucleome data collected from RAW264.7 cells at 20 hpi. Distributions of all proteins found in the lysatome (*x* axis) and nuclear fraction (*y* axis) (blue), and lysosomal hydrolases (red). Black broken line represents the line of best fit. *P* values, two-sided unpaired Wilcoxon rank-sum test. $n = 2$ biologically independent samples. **c**, Box plots displaying the relative fold-change (infected/uninfected) of membrane-bound lysosomal versus soluble lysosomal luminal proteins selected from the lysatome and nucleome samples, as per Fig. 1b, from $n = 2$ biologically independent samples. Box boundaries indicate the upper and lower interquartile range (IQR), the median is depicted by the middle boundary and whiskers represent 1.5× IQR.

linked to infection. We therefore set out to examine the significance of this organized re-trafficking of lysosomal proteases in more detail.

***STm* SPI-2 promotes high nuclear cathepsin activity.** To examine cathepsin localization and activity, we added a cell-permeable cathepsin reactive probe, DCG04-Bodipy-FLike (DCG04-FL), to live cells during *STm* infection. Analysis of nuclear extracts exhibited a striking increase in nuclear cathepsin activity during infection with wild-type *STm* compared with the uninfected control (Fig. 4a, right). Nuclear cathepsins were also of a higher molecular weight relative to their endolysosomal counterparts (Fig. 4a), which are processed to more active mature forms[14]. However, consistent with previous reports describing higher molecular-weight nuclear forms of cathepsins CtsB and CtsL[10,11,15], we too found these larger forms to be proteolytically active[10,15] because our probe binds only active enzymes. We verified that DCG04-FL does not cross-react with *STm* and that increased nuclear cathepsin activity does not lead to increased histone H3 cleavage, as previously reported (Extended Data Fig. 3a,b)[16]. Thus, newly synthesized active cathepsins are re-trafficked to the nucleus during *STm* infection.

Because the SPI-2 secretion system of *S*Tm has been implicated in re-trafficking of lysosomal contents to the external milieu[9], and nuclear cathepsin activity coincides with SPI-2-dependent proliferation (Extended Data Fig. 3a), we examined whether SPI-2 secretion is also required for nuclear cathepsin activity. Cathepsin activity in Tx-100-soluble lysates was comparable between RAW264.7 cells infected with wild-type, SPI-1 (Δ*prgK*) or SPI-2 (Δ*ssaV*) secretion system mutants (Fig. 4b, left). In contrast, nuclear cathepsin activity was reduced in cells infected with the SPI-2 mutant but not with the SPI-1 mutant (Fig. 4b, right). To test whether the trafficking of cathepsins to the nucleus is independent of their activity, we probed CtsB localization during infection when cells were treated with the CtsB and CtsL selective inhibitor, CA-074-Me. CtsB was trafficked to the nucleus during infection with wild-type *S*Tm independently of the presence of the inhibitor (Extended Data Fig. 3c). Thus, SPI-2 seems to promote active trafficking of cathepsins to the nucleus independently of cathepsin activity.

To ensure that our observations of SPI-2 promotion of nuclear cathepsin activity by SDS–polyacrylamide gel electrophoresis (SDS–PAGE) were not artefacts of biochemical fractionation, we used fluorescence microscopy to quantify nuclear cathepsin activity from single cells in situ (Fig. 4c,d). Wild type-infected cells exhibited increased nuclear cathepsin activity relative to uninfected bystanders (Fig. 4d). Furthermore, nuclear cathepsin activity in cells infected with the SPI-2-deficient mutant was reduced compared to wild type-infected cells (Fig. 4d). This increased cathepsin activity was within the nucleus (that is, cathepsin activity within the nuclear boundary as defined by Hoechst 33342-stained host nuclei) and the perinuclear region of wild type-infected cells, but not in uninfected bystanders, uninfected naïve or those infected with a SPI-2-deficient mutant (Fig. 4e). Of note, in some cases cells displaying elevated nuclear cathepsin activity exhibited a strong increase in cathepsin activity throughout the cell body (Fig. 4e, fifth image in first row) but, in general, the two metrics were not strongly correlated for cells with high nuclear cathepsin activity (Fig. 4f). Taken together, *S*Tm SPI-2 promotes the accumulation of molecularly distinct forms of cathepsins within the nucleus during infection.

Nuclear cathepsin activity correlates with signatures of cell death. To further examine the consequences of nuclear cathepsin activity, we extracted nuclei from cells treated with the cathepsin activity probe DCG04-Boclicky-TAMRA and analysed by flow cytometry. In cells exposed to wild-type *S*Tm, ~5.5% of nuclei were cathepsin positive compared to 1–1.5% exposed to the *ssaV* mutant (SPI-2) or heat-killed bacteria (Fig. 5a and Extended Data Fig. 4). A substantial fraction of cathepsin-positive nuclei was detected in the sub-G1 region of the fluorescence-activated cell sorting (FACS) plot (Fig. 5a and Extended Data Fig. 4), signifying DNA fragmentation occurring during pyroptotic cell death induced by *S*Tm infection[17,18]. *S*Tm lacking the SPI-2 secretion system and dead *S*Tm (both unable to proliferate intracellularly) elicited a residual amount of cathepsin-positive nuclei, in agreement with previous results (Fig. 4b,d). This residual non-SPI-2 effect is probably due to LPS.

To verify that cathepsins play a role in *S*Tm-induced cell death, we tested the impact of cathepsin inhibition on host cell death induced by *S*Tm by measuring lactate dehydrogenase (LDH) release[19]. Both wild-type *S*Tm and Δ*sifA* induced considerable levels of cell death at 19 hpi, with the latter exhibiting greater levels as expected (Fig. 5b). Cell death was largely dependent on the expression of a functional SPI-2 (Δ*ssaV*; Fig. 5b). Importantly, in all cases, cell death was partially inhibited by the addition of CA-074-Me (Fig. 5b). We further confirmed that CA-074-Me does not inhibit *S*Tm growth per se (Extended Data Fig. 5) and that it is selective against cathepsins, using two-dimensional thermal proteome profiling (2D-TPP)[20,21]. CA-074-Me specifically stabilized cysteine proteases cathepsins B, S, Z, F and K (Extended Data Fig. 6a and Supplementary Table 6), revealing a broader inhibitory spectrum for cathepsins than previously appreciated. Importantly, we found no evidence that CA-074-Me targets any other cysteine protease, including all caspases detected (Extended Data Fig. 6a)[22]. Because proteome

Fig. 4 | *S*Tm SPI-2 promotes nuclear cathepsin activity. a, Uninfected (–) and wild-type (WT) *S*Tm-infected RAW264.7 cells (MOI = 100:1) were treated with either the cathepsin 488-nm probe DCG04-FL (5 μM) or DMSO vehicle for 3 h before harvesting at 20 hpi. Such inhibitor-based probes covalently link to the reactive cysteine in the catalytic site of endolysosomal proteases, and thus the amount of bound probe directly corresponds to cathepsin activity[34]. Endosomal organelles containing active lysosomal cysteine proteases were effectively solubilized with the non-ionic detergent Tx-100, as evidenced by the presence of highly active mature cathepsins in cells treated with DCG04-FL (left), but not in DMSO-treated cells, thus demonstrating the specificity of the DCG04-FL probe. Cathepsin activity was elevated in the Tx-100-soluble fraction of infected relative to uninfected cells, particularly for CtsB and CtsZ (left). Tx-100-soluble (left) and -insoluble (right) extracts were separated by SDS–PAGE and then visualized using a fluorescence scanner (Excitation 405 nm/Emission 520 nm). Immunoblot with anti-GAPDH and Coomassie staining of histones were used as loading controls for lysatome and nucleome samples, respectively. Data are representative of two biological replicates (all blots shown in Supplementary Information). **b**, RAW264.7 cells infected with WT, Δ*ssaV* (SPI-2) or Δ*prgK* (SPI-1) *S*Tm were treated with DCG04-FL (5 μM) and lysatome (left), and nucleome (right) extracts were separated and visualized as described in **a**. Loading controls as in **a**. Data are representative of two biological replicates (all blots shown in Supplementary Information). **c**, DCG04-Boclicky-TAMRA (5 μM) was added to the media 2 h before harvesting at 2 hpi (upper) and 20 hpi (lower) (MOI = 100:1) of RAW264.7 cells with *S*Tm constitutively expressing GFP from pDiGc (see Methods). Cells were then fixed and stained with Hoechst 33342 (DNA) and images acquired using a ×20 objective. Scale bars, 50 μm. **d**, Violin plots of single-cell nuclear cathepsin activity quantified in RAW264.7 cells infected with WT or Δ*ssaV* (SPI-2) *S*Tm constitutively expressing GFP from pDiGc (MOI = 100:1) for 20 h. Infected cells were treated with DCG04-Boclicky-TAMRA 2 h before cell fixation. Nuclear cathepsin activity was measured by quantifying DCG04-Boclicky-TAMRA signal that overlapped with Hoechst 33342-stained nuclei. Each data point represents a measurement per cell nucleus, which was further classified as infected or uninfected bystander based on the presence or absence, respectively, of GFP-expressing *S*Tm located within the host cell perimeter. Nuclear cathepsin activity was normalized to nuclear area. Red bars, medians. A two-sided unpaired Wilcoxon rank-sum test was used to calculate *P*. *n* denotes the total number of single nucleus measurements from two biologically independent samples. **e**, Cathepsin activity in fixed cells, prepared as in **c**, was visualized by confocal microscopy. Depicted cells are representative of high and low nuclear cathepsin activity distributions in **d**. Cells with high nuclear and perinuclear cathepsin activity are more readily observed in cells infected with WT *S*Tm compared to those infected with Δ*ssaV* (SPI-2) mutants, uninfected bystanders and naïve cells from control wells not exposed to bacteria. To observe clear boundary definition between the nucleus and the non-nuclear area of the cell, single planes from a *z*-stack are displayed. Scale bars, 2 μm. **f**, Single-cell analysis of nuclear and non-nuclear cathepsin activity in RAW264.7 cells infected with WT *S*Tm for 20 h, as in **d**. Cells and nuclei were segmented using CellProfiler. Nuclear cathepsin activity was measured by quantifying DCG04-Boclicky-TAMRA signal overlapping with Hoechst 33342-stained nuclei. Non-nuclear cathepsin activity was calculated by subtracting nuclear cathepsin activity (TAMRA) from total TAMRA signal per cell. The upper 95th quantile (Q95) representing cells with the highest nuclear cathepsin activity ($n = 31$) was analysed by direct comparison with the corresponding non-nuclear cathepsin activity. The blue line represents a fitted linear regression model and *r* denotes Pearson correlation coefficient.

coverage for caspase-11 was incomplete, we used an in vitro assay to verify that CA-074-Me does not affect caspase-11 proteolytic activity (Extended Data Fig. 6b). Overall, these findings suggest that cathepsin-dependent cell death is promoted by *S*Tm escape into the cytoplasm and is required in conditions where caspase-11 is active.

Cathepsin activity is required for *S*Tm-induced caspase-11-dependent cell death. To further understand the role of specific host molecules, and to ensure that our observations go beyond RAW264.7 cells, which lack key inflammasome components[23], we sought to replicate our findings using bone marrow-derived macrophages (BMDMs) from rodent knockout

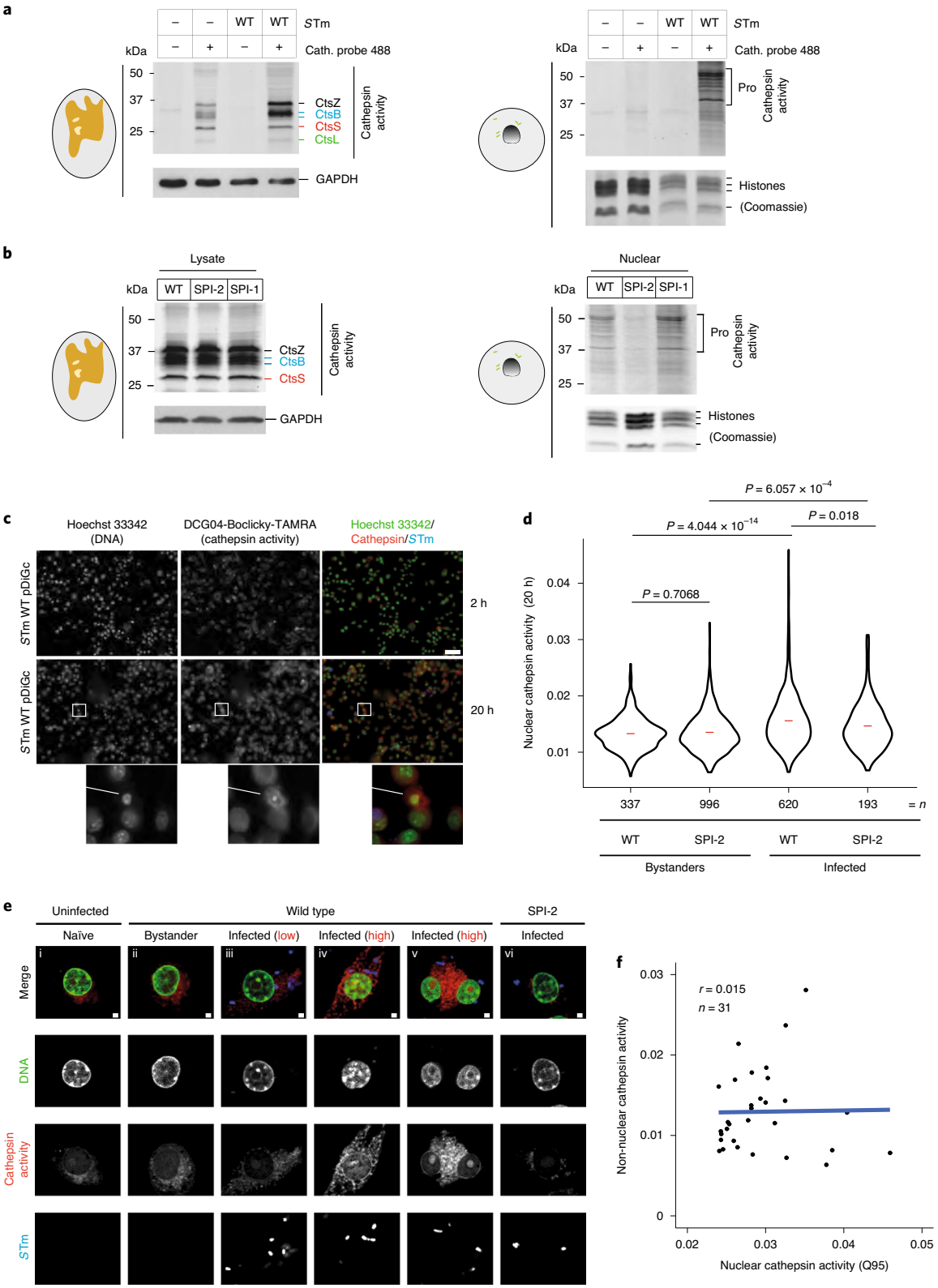

lines. Consistent with previous reports[24,25], LDH release started ~10 hpi (Fig. 5c). This LDH release was dose-dependently suppressed with CA-074-Me, similar to our observations in RAW264.7 cells.

Delayed lytic cell death of *S*Tm-infected macrophages is dependent on the cytoplasmic LPS sensor caspase-11 (ref. [2]). We therefore tested whether cathepsin-dependent cell death requires the presence of caspase-11. Cathepsin-dependent cell death required caspase-11 and occurred independently of the canonical inflammasome activators NLRP3 and NLRC4 (Fig. 5d). To test whether cathepsin activity is required for canonical inflammasome-mediated cell death, we infected BMDMs with SPI-1 expressing *S*Tm (that is, SPI-1(ON)), which is known to rapidly trigger the canonical inflammasome[26]. In this case, we observed no impact of cathepsin activity on SPI-1-induced cell death (Extended Data Fig. 7). These data demonstrate that cathepsins play a specific functional role in non-canonical inflammasome activation.

Cathepsin activity functions downstream of LPS-triggered caspase-11 activation. To examine whether cathepsin activity is required upstream or downstream of caspase-11 activation, we transfected LPS into the host cytoplasm to directly activate the non-canonical inflammasome. Remarkably, direct caspase-11 activation with cytoplasmic LPS was inhibited by CA-074-Me (Fig. 5e) and, on its own, promoted nuclear cathepsin activity (Extended Data Fig. 8), demonstrating that the cathepsin activity required for cell death functions downstream of caspase-11 activation. Consistently, caspase-11 activation during wild-type *S*Tm infection was unaltered by CA-074-Me (Extended Data Fig. 9). Thus, LPS per se can trigger relocation and/or activation of cathepsins in the nucleus, consistent with the basal signal we observed with intracellular non-proliferating *S*Tm (Figs. 4b,d and 5). This suggests that cathepsin-dependent cell death is a host-induced process and that cathepsin activity is required for non-canonical inflammasome activation.

Cathepsin activity promotes gasdermin D expression. Our previous experiments suggested that cathepsin activity is required downstream of caspase-11. The only known target of caspase-11 is gasdermin D (GSDMD). In our 2D-TPP data, CA-074-Me led to a strong decrease in GSDMD expression in a dose-dependent manner in RAW264.7 cells (Fig. 6a). We verified that this occurs also in BMDMs, by measuring GSDMD levels during infection. An infection-dependent increase in GSDMD abundance could be suppressed by the addition of CA-074-Me (Fig. 6b). In addition, CA-704-Me broadly reduced the abundance of several pro-inflammatory proteins, including IL-1b, IL-18, IL-1a, GBP1 GBP2, GBP4, GBP5, GBP7, GBP9, IFI202, IFI204, ISG20 and ISG15 (Extended Data Fig. 6c and Supplementary Table 6). Taken together, we consider that nuclear cathepsin activity results in increased levels of GSDMD and pro-inflammatory proteins, and hence contributes to non-canonical inflammasome-mediated cell death.

Nuclear cathepsin activity is required for *S*Tm-induced cell death. To address which cellular compartment cathepsin activity is required for cell death, we followed a two-pronged approach. First, we hypothesized that if the suppression of *S*Tm-induced host cell death by cathepsin inhibition can be explained by cathepsin inhibition in the SCV and thereby SPI-2 activation and *S*Tm proliferation, then addition of cathepsin inhibitors subsequent to the initiation of SPI-2-dependent replication should abrogate their ability to inhibit host cell death. However, addition of inhibitor at 8 hpi rescued cathepsin-dependent cell death in BMDMs to a similar degree compared to addition of CA-074-Me at the beginning of infection (Fig. 6c). These data are consistent with a role for late cathepsin activity in promoting caspase-11-mediated cell death. Since cathepsins relocate to the nucleus at this time point, we reasoned that these activities play a role in driving cell death.

Second, we generated immortalized macrophages (iMACs) overexpressing the endogenous cathepsin inhibitor stefin B with or without a nuclear localization sequence (NLS) (Fig. 6d and Extended Data Fig. 10). We then infected stefin B-expressing cells with wild–type *S*Tm and measured LDH release. In this case, nuclear-targeted stefin B partially suppressed LDH release in a dose-dependent manner (Fig. 6e). This effect was specific to nuclear-targeted, and not to cytoplasmic, stefin B (Fig. 6e). Overall, these results are consistent with a specific functional role for nuclear cathepsin activity in promoting non-canonical inflammasome activation.

Discussion

We quantified the host pool of newly synthesized proteins, enabling unprecedented proteome-wide spatiotemporal resolution of a

Fig. 5 | Cathepsin activity promotes *S*Tm-induced caspase-11-dependent cell death. a, Nuclei were extracted from RAW264.7 cells treated with DCG04-Boclicky-TAMRA (5 μM) for 2 h before harvesting at 20 hpi with wild-type (WT), a SPI-2 mutant (Δ*ssaV*) or heat-killed WT bacteria (HK WT) (MOI = 100:1). Formaldehyde-fixed nuclei were subsequently counterstained with Hoechst 33342 and analysed by flow cytometry. Cells in the G1, S or G2 phase of the cell cycle are separated by Hoechst 33342 staining on the *x* axis. Cathepsin activity (DCG04-Boclicky-TAMRA) is indicated by the percentage of total DCG04-Boclicky-TAMRA-positive nuclei in either sub-G1 or G1/S/G2, or the combined total of sub-G1 and G1/2/G2. Data combining all biological replicates from two independent experiments can be seen in Extended Data Fig. 4. **b**, Pyroptotic cell death was assessed by quantifying LDH release into culture supernatants of RAW264.7 cells infected with WT, SPI-2 (Δ*ssaV*) or the effector deletion (Δ*sifA*) mutants in the presence of 25 μM CA-074-Me or DMSO solvent control at 19 hpi. The Δ*sifA* mutant has a strong replication defect and readily escapes into the cytoplasm, hyperactivating caspase-11-dependent cell death[5]. *n* denotes biologically independent samples combined from three independent experiments (batches), each batch containing a minimum of four biological replicate wells per condition. Data represent percentage LDH release per condition relative to maximum LDH release (see Methods). Box plots are depicted as in Fig. 3c. An unpaired *t*-test (two-sided) was used to calculate *P*. **c**, BMDMs were infected with wild-type *S*Tm (MOI 100:1), followed by incubation in the presence of the cathepsin inhibitor CA-074-Me at the indicated concentrations. At the indicated hpi times, cell death was measured as the percentage of LDH released into culture supernatants. Data points represent the mean, and error bars indicate the 95% confidence interval. *n* denotes biologically independent samples. Time points 0, 10 and 14 h are derived from three biological replicates per condition ($n = 3$ per condition) from a single batch, whereas the 18-h time point contains combined data from three or more independent experiments (batches), each batch containing three or four biological replicates per condition (DMSO, $n = 30$; CA-074-Me (12.5 μM), $n = 28$; CA-074-Me (25 μM), $n = 13$). **d**, Related to **a**: WT, caspase-11$^{-/-}$, NLRP3$^{-/-}$ and NLRC4$^{-/-}$ BMDMs were infected with WT *S*Tm (MOI = 100:1), followed by incubation in the presence of CA-074-Me (12.5 μM) 18 hpi. The percentage of LDH released into culture supernatants was measured at 18 hpi. *n* denotes biologically independent samples combined from >3 (WT) and 3 (mutant genotypes) independent experiments (batches), each batch containing two to four biological replicates per condition. A two-sided unpaired *t*-test was used to calculate *P*. **e**, RAW264.7 cells were transfected with LPS with Fugene (Promega) for 20 h. Pyroptotic cell death was assessed by quantifying LDH release into culture supernatants in the presence of 25 μM CA-074-Me relative to a DMSO solvent control. *n* denotes biologically independent samples combined from three independent experiments (batches), each batch consisting of a minimum of three biological replicate wells per condition. Box plots are depicted as in Fig. 3c. A two-sided unpaired *t*-test was used to calculate *P*.

host–pathogen interface. This dataset provides a rich resource for infection biology, and could serve as a basis for new hypotheses. We used it to reveal a role for cathepsins in activating *S*Tm-induced pyroptosis via the non-canonical inflammasome. This proof of principle illustrates how the selective quantification of the newly synthesized host proteome within different cellular compartments can illuminate mechanisms that would otherwise remain hidden using conventional proteomic approaches.

The host proteome during *S*Tm infection has been mapped previously: whole-proteome analysis during infection of RAW264.7

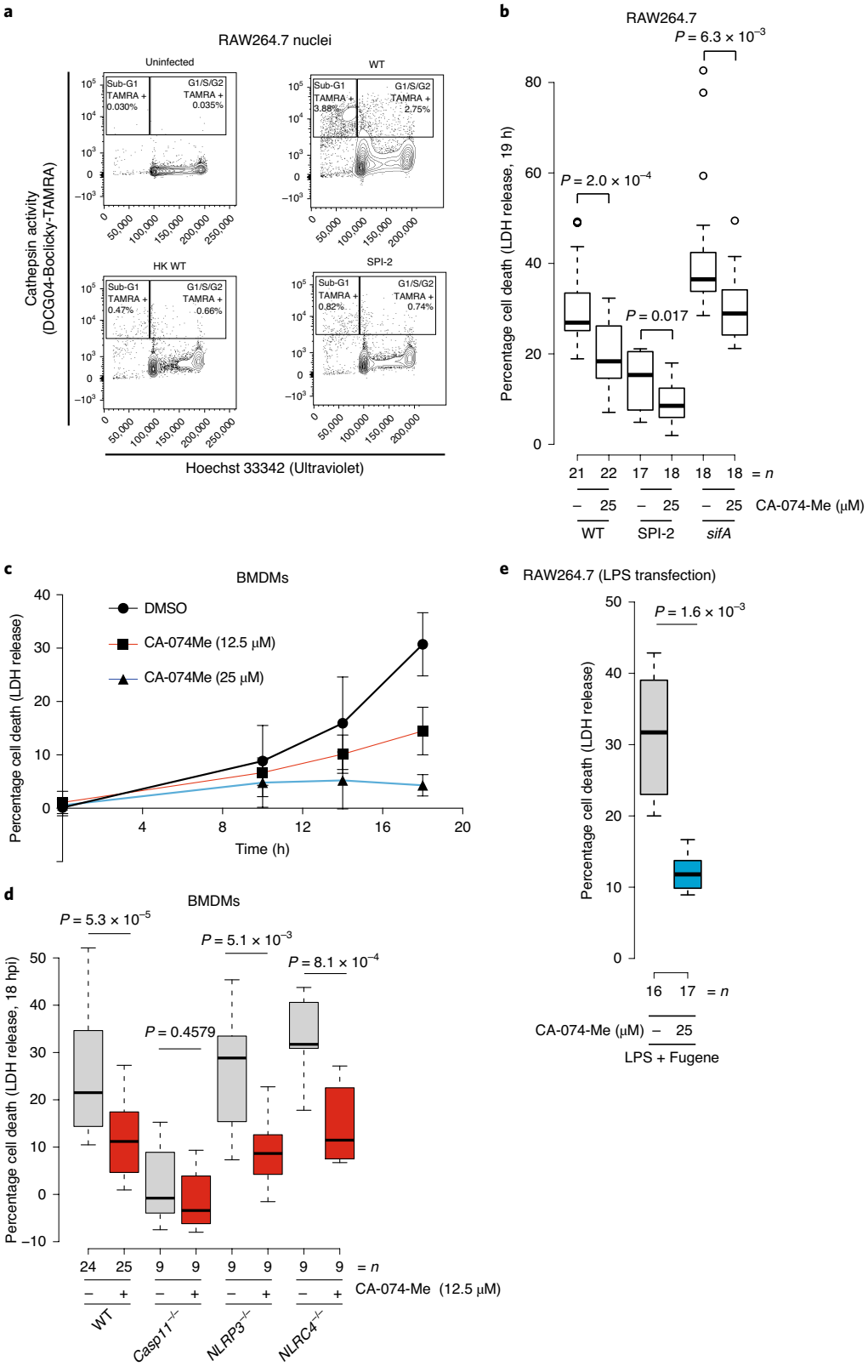

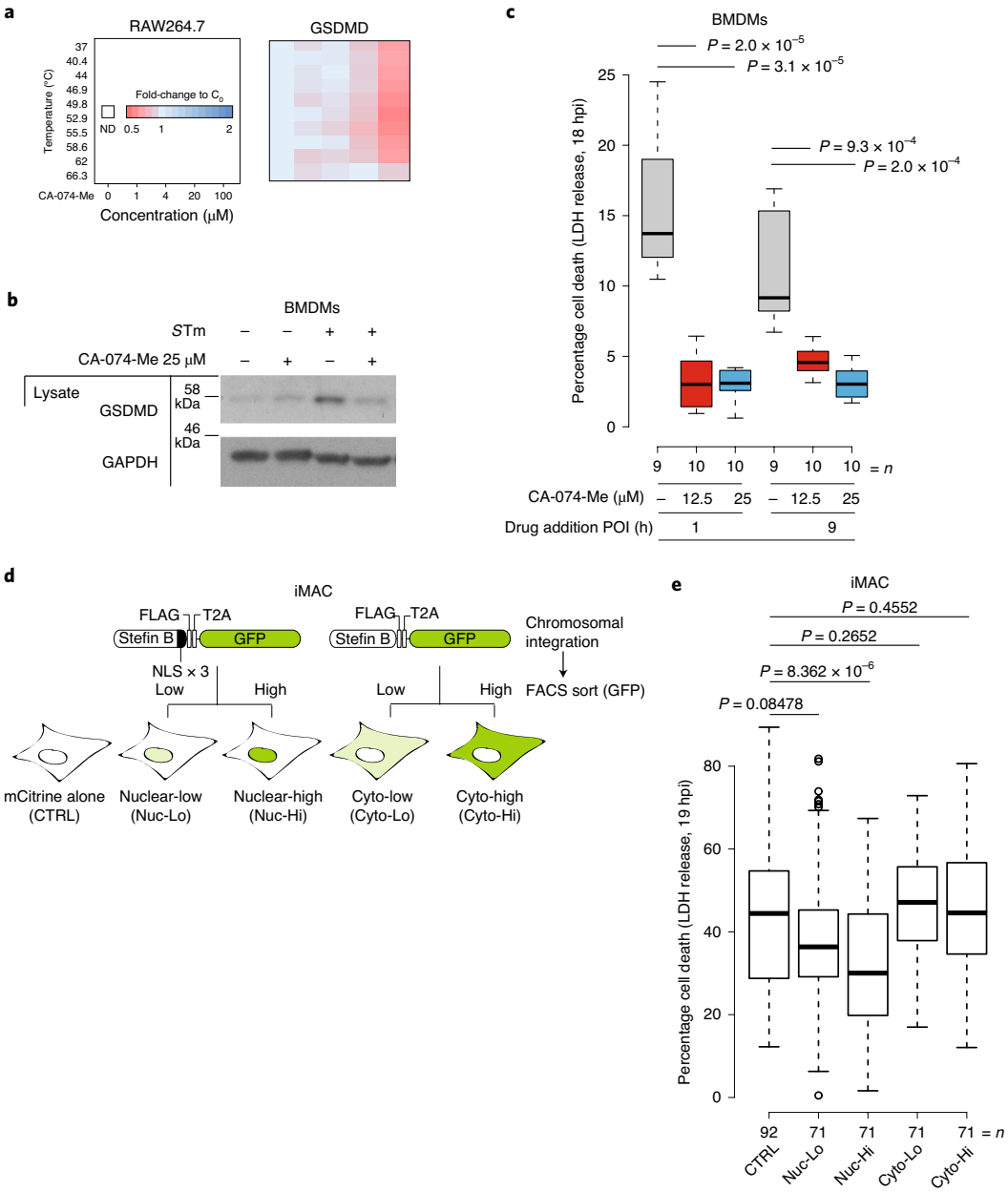

Fig. 6 | Cathepsin activity promotes GSDMD expression and its nuclear activity is required for cell death. a, 2D-TPP of RAW264.7 cells infected with wild-type *STm* for 20 h in the presence of increasing concentrations of CA-074-Me post *STm* uptake. Heatmap of GSDMD shows decreased abundance (evident from decrease in protein abundance at lower temperatures, before protein melts) with increasing CA-074-Me concentrations. The key is presented to the left of the heatmap; for each protein and temperature, the signal intensity was normalized to the DMSO vehicle control (CTRL). 2D-TPP data can be found in Supplementary Table 6 and Extended Data Fig. 6. **b**, BMDMs were infected with wild-type *Salmonella* 14028s (20 hpi) and cell lysates analysed by immunoblot for GSDMD and GAPDH as a loading control. A replicate blot from an independent experiment can be found in the Supplementary Information. **c**, BMDMs infected with wild-type *STm* (MOI = 100:1) were treated with either CA-074-Me (12.5 or 25 μM) or DMSO control at 1 or 9 hpi. Box plots are depicted as in Fig. 3c. A two-sided unpaired *t*-test was used to calculate *P*. *n* denotes the combined data from three independent experiments (batch), each batch containing three or four biological replicates per condition. POI, post-infection. **d**, Schematic depicting stefin B constructs used to generate iMAC cell lines targeting stefin B to the nucleus (Nuc) with 3 × NLS or expressed in the cytoplasm (Cyto). Stefin B potently inhibits several cathepsins (for example, CtsL, CtsS, CtsH and, to a lesser extent, CtsB)[35] and has previously been used to block cathepsin activity and overcome cathepsin redundancy[36]. Retrovirally transduced iMACs were FACS sorted for low (Lo) or high (Hi) expression of stefin B fusion proteins, which was then verified by both immunoblot (Extended Data Fig. 10a) and localization of the stefin B fusion protein by microscopy (Extended Data Fig. 10b). We tested the sensitivity of stefin B-expressing cells to conditions known to activate the canonical inflammasome (that is, nigericin + LPS) and the lysosome-destablizing agent, LLoMe, which triggers a distinct form of cell death. In line with our previous observations that cathepsin activity is not required for canonical inflammasome activation, cells with nuclear-expressed stefin B were refractory to nigericin + LPS treatment, but also to LLoMe-induced cell death (Extended Data Fig. 10c,d). **e**, iMACs expressing stefin B targeted to the nucleus, or expressed in the cytoplasm, were infected with wild-type *STm* (MOI = 100:1; 19 hpi). LDH release was quantified as in Fig. 5b. Sample labels are as described in **d**. Box plots are depicted as in Fig. 3c. A one-sided unpaired *t*-test was used to calculate *P*. *n* denotes the combined data from four independent experiments (batches), each batch containing more than eight biological replicates per condition.

macrophages (at the time, the authors could identify in total ~1,000 host proteins)[27], and mapping the secretome of human monocytes (THP-1) during early stages of infection—before intracellular SPI-2-dependent proliferation[28]. In contrast to previous studies, our approach has three advantages: (1) we monitor dynamic host proteome responses, collecting samples at different phases of infection and quantifying the newly synthesized proteins at each stage; (2) we use subcellular fractionation and pulsed stable isotope labelling of amino acids-azidohomoalanine (pSILAC-AHA) to assess protein redistribution between cellular compartments, quantifying 4,978 newly synthesized host proteins from the cytoplasm/organelles, the nucleus and the extracellular milieu (lysatome, nucleome and secretome); and (3) we deconvolute the *S*Tm-specific response by direct comparison of our data with similarly acquired data on the macrophage response to LPS[8].

We observed that lysosomal proteases are rewired in their cellular trafficking during *S*Tm infection, both to the extracellular space and the nucleus (Supplementary Discussion). Support for nuclear cathepsins playing an active role in cell death comes from previous observations that CtsB is delivered to the nucleus during bile salt-induced apoptosis. In this case, addition of CA-074-Me or silencing of *ctsB* expression abrogated cell death[29]. Cathepsin B can also induce nuclear apoptosis in digitonin-permeabilized cells[30]. Moreover, deletion of the endogenous cathepsin inhibitor stefin B led to enhanced caspase-11 transcription in BMDMs[31]. Albeit in the absence of infection, these findings provide strong support that nuclear cathepsins play an active role during cell death. Consistently, we observed an increase in nuclear localization of CtsA, CtsB, CtsL, CtsS, CtsD and CtsZ during *S*Tm infection, which correlated with signs of cell death such as DNA fragmentation. Furthermore, we could (1) inhibit pyroptosis by the addition of CA-074-Me 8 hpi when cathepsin activity is present in the nucleus; and (2) partially inhibit cell death by expressing nuclear, but not cytosolic-targeted, stefin B. Both are consistent with nuclear cathepsin activity playing an active role in *S*Tm-induced cell death. By direct activation of caspase-11 through transfection of LPS into the host cytoplasm, we demonstrate that cathepsin activity is required downstream of caspase-11 activation. We observed elevated GSDMD expression during *S*Tm infection in a cathepsin-dependent manner. Because GSDMD is the only known downstream substrate of caspase-11, and is essential for execution of cell death via the non-canonical inflammasome, our current working model entails LPS-driven translocation of cathepsins to the nucleus to promote GSDMD expression and thereby to impact non-canonical inflammasome activation.

In summary, we used a proteomics approach to selectively enrich and quantify newly synthesized host proteins during *S*Tm infection, unmasking a hidden layer of the mammalian innate immune response. This rich tapestry of regulated proteins, resolved throughout time and space, offers a resource for new hypotheses governing host–pathogen interactions. We provide a proof of principle by further interrogating the re-trafficking of cathepsins outside of the cell and into the nucleus during *S*Tm infection. This highlights a role for cathepsins during infection and adds a new layer of complexity to *S*Tm-induced pyroptosis.

Methods

No statistical methods were used to predetermine sample size

Media, chemicals and reagents. The following chemicals and reagents used were purchased from Sigma: dimethylsulfoxide (DMSO; catalogue no. D8418), L-methionine, L-cysteine, L-lysine, L-arginine and L-glutamine. Tris(carboxyethyl) phosphine (catalogue no. C4706) and 40 mM 2-chloroacetamide (catalogue no. 22790), Triton X-100 (catalogue no. X100), heat-inactivated foetal bovine serum (FBS) (no. F9665-500ML), phalloidin-ATTO 700 (no. 79286-10NMOL), gentamicin (no. G1914), DMEM 4.5 g l^{-1} glucose (no. 41965), DMEM 4.5 g l^{-1} glucose non-GMP formulation (no. ME 100073L1, without L-lysine HCl and L-arginine HCl), dialysed FBS (no. 26400044) and RPMI 1640 without (no. 11835-030) and with (no. 52400-025) phenol red, respectively, were purchased from Gibco. DMEM (containing high glucose) and HEPES (buffered and without phenol) were purchased from Thermo Fisher Scientific (no. 21063029). Cathepsin inhibitor CA-074-Me was purchased from EMD Millipore (no. 205531), AHA from Click chemistry tools (no. 1066-100), cOmplete mini EDTA-free protease inhibitors from Roche (no. 11873580001), recombinant murine M-CSF from PeproTech (no. 315-02), Hoechst 33342 from Life Technologies (no. H3570), formaldehyde 16% (w/v) from Thermo Scientific Pierce (no. 28908) and the CytoTox 96 Non-Radioactive Cytotoxicity kit from Promega (no. G1780). Antibodies were mostly purchased from Cell Signalling: GAPDH(D16H11) (catalogue no. 8884), histone H3(D1H2) (catalogue no. 4499 P, Sigma(Merck); anti-rabbit HRP (Sigma/GE, no. NA934-1ML), M2 antibody (no. F3165), anti-mouse HRP (Sigma, no. HVZ-A4416-1ML) and anti-Lamin A (Sigma, no. SAB4501764). Anti-RNA polymerase Sigma 70 (RpoD) (2G10, catalogue no. GTX12088) was purchased from Acris Antibodies. Anti-caspase-11 was purchased from Novus Biological (17D9, catalogue no. NB120-10454SS). Anti-GSDMD was purchased from Abcam (catalogue no. ab209845). Cathepsin B antibody was purchased from R&D systems (no. AF965-SP). Anti-mouse Alexa Fluor plus 647 antibody was purchased from Thermo Fisher Scientific (catalogue no. A32728). Anti-tubulin (no. 926-42211) was purchased from Li-Cor. Mouse serum was purchased from Abcam (no. ab7486).

Bacterial culture conditions and strain construction. *S*Tm was cultured at 37 °C in lysogeny broth (LB, Lennox) with agitation overnight in the presence of antibiotics for plasmid selection when necessary. Strains expressing antibiotic resistance genes were selected and maintained on solid LB agar plates containing citrate and either 30 μg ml^{-1} kanamycin (mutant selection) or 100 μg ml^{-1} ampicillin (for pDiGc and pFCcGi plasmids). Mutant strains were retrieved from a single-gene mutant collection[37], followed by PCR confirmation and re-transduction of the mutated loci into the wild-type *S*Tm 14028 background using the P22 phage. To visualize bacteria during infection using fluorescence microscopy, a plasmid constitutively expressing green fluorescent protein (GFP), GFP-pDiGc[38] or mCherry-pFCcGi, was introduced into bacteria by electroporation followed by selection on LB agar containing ampicillin 100 μg ml^{-1} at 37 °C.

Cell culture conditions. RAW264.7 cells (ATCCTIB71^{T}) purchased from ATCC were routinely cultured in DMEM containing 4.5 g l^{-1} glucose and passaged by detaching with accutase (StemCell, no. A1110501). RAW264.7 cells were routinely tested for *Mycoplasma* using the MycoAltert Mycoplasma detection kit (Lonza, no. LT07-118), which consistently returned a negative result. Only cells below passage no. 15 were used for experiments. Bone marrow was isolated from both male and female 8–12-week-old mice from wild-type C57Bl/6 mice, and Casp1/11$^{-/-}$ (ref. [39]), Casp11$^{-/-}$ (ref. [40]), Nlrp3$^{-/-}$ (ref. [41]) and Nlrc4$^{-/-}$ (ref. [42]) (C57BL/6 genetic background) from ETH. Femur and tibia were flushed with PBS. Bone marrow cell suspension (from femur) was filtered through a 70-μm cell strainer (Falcon), washed with 20 ml of PBS, spun down at 1,200 r.p.m. (4 °C, 15 min) and resuspended in 1 ml of 90% heat-inactivated FBS (Life Technologies) + 10% DMSO (Sigma) at a concentration of 1×10^7, then transferred to liquid nitrogen for storage. For experiments, bone marrow was thawed and washed in 10 ml of pre-warmed RPMI supplemented with 10% FBS (Sigma) (RPMI + FBS). Cells were then resuspended in 20 ml of RPMI + FBS without phenol, supplemented with 50 μg ml^{-1} gentamicin and 40 ng ml^{-1} macrophage-stimulating factor (M-CSF). M-CSF was reconstituted in 0.1% bovine serum albumin (Carl Roth, catalogue no. 8076.4), then aliquoted and stored at −30 °C. Cell suspensions were then split across two 10-cm Petri dishes and incubated at 37 °C, 5% CO_2 for 6 d to allow BMDM differentiation. BMDMs were washed with 3 ml of PBS and detached by incubation of cells in 3 ml of cell dissociation buffer (5% FBS, 2.5 mM EDTA in PBS) and incubation on ice for 5 min. Resuspended BMDMs were pooled, pelleted at 500*g* and resuspended in 20 ml of RPMI + FBS (5%) without phenol and supplemented with 40 ng ml^{-1} M-CSF.

Proteomic sample preparation. RAW264.7 cell infections were performed as previously described[43]. Approximately 18–20 h before infection, RAW264.7 cells were seeded in DMEM containing 10% FBS (DMEM + FBS) at a cell density of 0.9×10^5 per well in six-well plates. Cell density from overnight cultures of wild-type *S*Tm 14028 s expressing mCherry from pFCcGi grown in LB Broth (Lennox) at 37 °C was measured (OD_{578}) and normalized to $OD_{578} = 1$. Cells were then washed in PBS and pelleted at 8,000*g* for 5 min. To opsonize bacteria, pellets were resuspended in DMEM containing 10% mouse serum and incubated at room temperature for 20 min. Opsonized bacteria and mock inoculum were added directly to wells containing RAW264.7 cells at a multiplicity of infection (MOI) of 100:1 and centrifuged at 170*g* for 5 min to promote bacterial uptake. Infected cells were incubated at 37 °C under 5% CO_2 for 25 min. Infected cells were then washed once with media and replaced with DMEM + FBS containing 100 μg ml^{-1} gentamicin and returned to the incubator for 1 h. Media was then replaced with DMEM + FBS containing 16 μg ml^{-1} gentamicin for the remainder of the experiment; this step denotes $t = 0$ h. Therefore, for all experiments, t denotes time since addition of DMEM + FBS containing 16 μg ml^{-1} gentamicin.

To quantify the sub-population of host proteins synthesized within a specific time frame, we simultaneously pulsed cells with stable isotope labelling by/with amino acids in cell culture (SILAC) and an azide-containing analogue of methionine (AHA). Intermediate or heavy SILAC labels facilitated robust protein

quantification relative to uninfected controls, whereas AHA enabled enrichment of the newly synthesized proteome. These amino acid labels can be used as substrates by the host's endogenous translational machinery and are thereby incorporated into newly synthesized proteins (pSILAC-AHA). Cells were pSILAC-AHA labelled as previously described[6] with the following modifications. To deplete cells of methionine, lysine and arginine, roughly 3.5 h before harvest infected and corresponding control cells were washed three times with pre-warmed PBS followed by 30-min incubation in DMEM dropout media: DMEM containing 10% dialysed FBS, 4.5 g l^{-1} glucose, 40 mM L-glutamine, 60 µg ml^{-1} L-cysteine and 16 µg ml^{-1} gentamicin, but lacking L-methionine, L-lysine and L-arginine (Gibco). This was then replaced with DMEM dropout media supplemented with 100 µM AHA and either 84 µg ml^{-1} [$^{13}C_6$,$^{15}N_4$]L-arginine and 146 µg ml^{-1} [$^{13}C_6$,$^{15}N_2$]L-lysine (heavy) or 84 µg ml^{-1} [$^{13}C_6$]L-arginine and 146 µg ml^{-1} [4,4,5,5-D_4]L-lysine (intermediate) SILAC labels (Cambridge Isotope Laboratories). Cells were then pulse-labelled for 3 h to allow sufficient time for protein translation and subsequent trafficking throughout the cell.

For cell fractionation, conditioned media containing the secretome from pSILAC-AHA-labelled cells were collected as previously described[6] and stored at −80 °C. RAW264.7 cells were then washed three times with pre-warmed PBS followed by partial lysis in 1 ml of PBS containing 0.1% Tx-100 and protease inhibitors (Roche, cOmplete, mini, EDTA-free) per well for 10 min at room temperature. Intermediate and heavy isotopically labelled samples corresponding to either infected or uninfected cells were combined in a 1:1 ratio. To isolate Tx-100-resistant nuclei and bacteria, the lysate was centrifuged at 3,220*g* for 10 min at 4 °C. Supernatant containing the lysatome was transferred to a separate tube, and the pellets containing the nucleome were washed with PBS containing 0.1% Tx-100, followed by storage at −80 °C. Thus, the lysatome is a nuclear-free cell lysate.

To provide enrichment for the newly synthesized proteome, samples from two biological replicates simultaneously pulse-labelled with SILAC and AHA (biological replicates contained reversed SILAC labels) for 3 h before harvest were harvested as previously described[8], with the following modifications. Secretome and lysatome samples were thawed and concentrated to a volume of ~250 ul using a 15-ml Amicon Ultra centrifugal device with a 3-kDa cut-off at 4 °C and 3,220*g*. The nucleome pellet was thawed and solubilized in Lysis buffer (Thermo Fisher Scientific, Click-iT, no. C10416) followed by DNA shearing using a probe sonicator. Newly synthesized proteins were then enriched using 100 ul of beads and, according to the manufacturer's instructions, with the following modifications. Newly synthesized AHA-containing proteins were reacted with beads overnight (~16 h) at room temperature with rotation, and samples were then centrifuged at 2,600*g*. Beads were then washed three times with SDS buffer (1% SDS, 100 mM Tris pH8, 5 mM EDTA and 500 mM NaCl) followed by reduction and alkylation by resuspending the beads in 500 ul of SDS buffer containing 10 mM Tris(carboxyethyl)phosphine (Sigma, no. C4706) and 40 mM 2-chloroacetamide (Sigma, no. 22790). Samples were then incubated for 30 min at 37 °C with constant agitation at 1,000 r.p.m. Beads were transferred to retention columns and washed in the following sequence: seven times with 1 ml of SDS wash buffer, ten times with 1 ml of freshly prepared urea buffer (8 M urea, Tris-HCl pH 8.0), ten times with 20% 2-propanol and ten times with 20% acetonitrile. Beads were then transferred to low-protein-binding tubes by resuspending in buffer containing 100 mM Tris pH 8.0, 2 mM $CaCl_2$ and 4% acetonitrile. Beads were then centrifuged at 2,600*g* for 1 min and the supernatant decanted.

For peptide preparation, on-bead digestion was carried out in 50 ul of digestion buffer (8 M urea, Tris-HCl pH 8.0, 2.5% acetonitrile) by the addition to each tube of 2 µl of 0.5 µg µl^{-1} LysC/trypsin and incubation at 37 °C for 4 h with shaking at 1,000 r.p.m. Urea was then diluted by the addition of 150 µl of buffer (100 mM Tris pH 8.0, 2 mM $CaCl_2$ and 4% acetonitrile) and incubation overnight at 37 °C. Supernatants were then transferred to fresh microfuge collection tubes, and beads were washed with 200 µl of H_2O to collect residual peptides and collated. Samples were acidified by the addition of 8 µl (2% of the sample volume) of 10% formic acid followed by acidification verification using a pH strip.

Peptides were desalted by binding to a Waters Oasis HLB 96-well µElution Plate (Waters, no. 186001828BA) using a vacuum manifold. Wells were pre-conditioned by the passage of 100 µl of 100% acetonitrile followed by 100 µl of Oasis buffer B (1% formic in 60% MeOH), then 100 µl of Oasis buffer A (1% formic in H_2O). Samples were then bound followed by sequential washes with 300, 200 and 100 µl of Oasis buffer A. To elute peptides, a collection tray was loaded with glass vials over which the Oasis plate was carefully aligned. Peptides were eluted subsequently in 50 and 25 µl of Oasis buffer B. Glass vials were then transferred to 2-ml centrifuge tubes, pulse-spun stored at −20 °C. Secretome and nucleome fractions were evaporated using a speedVac at 35 °C for ~2 h, then resuspended in 20 µl of injection buffer (96.9% water, 3% acetonitrile and 0.1% formic acid) for direct analysis by nano liquid chromatography–tandem mass spectrometry (LC–MS/MS) on a Velos Orbitrap.

To reduce sample complexity, lysatome samples were subjected to high-pH, reversed-phase fractionation. In brief, fractionation was performed on an Agilent 1260 high-performance liquid chromatography (HPLC) system equipped with a variable-wavelength detector (254 nm). For HPLC, fractionation was performed on an XBridge BEH C18 column (1 × 100 mm^2, 3.5 µm, 130 Å, Waters). Elution was performed at a flow rate of 0.1 ml min^{-1} using a gradient of mobile phase A (20 mM ammonium formate, pH 10) and phase B (acetonitrile), from 1 to 37.5% over 61 min. Fractions were collected every 2 min across the entire gradient length and concatenated into eight final samples, as discussed previously[44]. Fractions were dried in a SpeedVac and reconstituted in 0.1% formic acid before desalting on an Oasis Elution plate and analysis by LC–MS/MS. Samples were then analysed on an Orbitrap Velos Pro (Thermo Fisher Scientific) as previously described[8].

For proteomic data analysis, the raw data obtained by Orbitrap mass spectrometry were processed using MaxQuant software (v.1.5.0.0). The MaxQuant implanted search engine Andromeda was used to search MS/MS spectra against a mouse database obtained from Uniprot. In this database, the sequences of frequently observed contaminant proteins and the reversed sequences of all entries were included, to indicate the false-positive search hints. Trypsin/P was chosen as the digestion enzyme, and no more than two miss cleavages were allowed for peptide identification. Cysteine carbamidomethylation was used as the only fixed modification, while methionine oxidation, N-terminal acetylation and AHA replacement of methionine were chosen as the variable modifications. The minimal peptide length was set to seven amino acids. The mass tolerance for peptides was 20 ppm in the initial search and 6 ppm in the main search. The maximal tolerance for fragment ion identification was 0.5 Da. False discovery rates for the identification of proteins and peptides were set to 1%. The minimal unique peptide number for protein identification was set to 1%. At least two ratio counts (quantified peptides for each protein) were set for protein quantification. The 'requantify' and 'match between runs' were functionalized in MaxQuant. In the pSILAC-AHA samples, only protein groups having a ratio of >20% identified peptides containing medium or heavy labels were kept for further analysis. Proteins identified as potential contaminants, with reverse sequences and from only peptides, were removed. Average protein ratios were calculated only if they were quantified in both biological replicates. The data are available at ProteomeXchange[45] with the identifier PXD010179. Proteomic data were visualized using R (v.1.0.143) and Cytoscape (v.3.3.0). Heatmaps were visualized with Heatmapper[46].

Cytokine and chemokine quantification. RAW264.7 cells were infected with wild-type *S*Tm as described above, except that DMEM 4.5 g l^{-1} glucose-containing 0.2% FBS was used for 20-h incubation with 16 µg l^{-1} gentamycin. After 20 h, conditioned media were collected and centrifuged at 2,000 r.p.m. at 4 °C for 10 min. Supernatants were then frozen at −80 °C until analysis. Samples were analysed using a custom Quantibody Mouse Cytokine Antibody Array (protocol no. 061219 Cust-M7 SA14; test procedure no. SOP-TF-QAH-001, SOP-TF-QAH-003) from RayBiotech.

Flow cytometry of extracted nuclei. Infections were prepared as described above. Heat-killed *S*Tm inoculum was prepared by heating bacteria to 65 °C for 15 min before infection. Tissue culture media from infected cells were replaced with fresh DMEM containing 5 µM DCG04-Boclicky-TAMRA, followed by incubation for 1 h at 37 °C, 5% CO_2. Cells were washed three times in PBS followed by solubilization in 0.1% Triton X-100. Nuclei were pelleted (500*g*, 3 min), washed and resuspended in PBS containing 0.1% Tx-100. Nuclei were then fixed by the addition of formaldehyde to 4% wt/vol (Thermo Fisher Scientific, no. 28908) and incubated for 15 min at room temperature. Before flow cytometry, nuclei were stained with 2 µg ml^{-1} Hoechst 33342. Nucleus samples were acquired on a BD LSRFortessa (BD Biosciences) equipped with five lasers. Hoechst 33342 was excited by the 355-nm laser line, and fluorescence signal was collected using a 450/50 bandpass filter; TAMRA was excited by the 561-nm laser line and collected using a 585/15 bandpass filter. Doublets were carefully excluded by plotting Hoechst 33342 area versus width; nuclei with increased width signal were not considered. Post-acquisition analysis was done in FlowJo software (BD Biosciences).

SDS–PAGE and immunoblot. RAW264.7 cells and BMDMs were infected in six-well tissue culture plates at an MOI of 100:1, as described above. For BMDM immunoblots, cell lysates were harvested by washing twice with PBS and then partially lysing in 200 µl of PBS lysis buffer (PBS containing 0.1% Tx-100 and cOmplete mini EDTA-free protease inhibitors) on ice for 10 min. Nuclei were removed by centrifugation at 500*g* for 5 min. Supernatants were added to Laemmli buffer loading dye, heated to 95 °C for 3 min and analysed by immunoblot. To visualize cathepsin activity, infected and mock-treated cells were labelled with 5 µm DCG04-FL (λexcitation 488 λemission 520) 3–4 h before harvest. Cells were then washed three times with PBS and partially lysed in 200 µl of PBS lysis buffer on ice for 10 min. Cell lysates were then collected and nuclei pelleted at 50*g* for 3 min, followed by a subsequent spin at 500*g* to pellet bacterial cells. Nuclei and bacterial-enriched pellets were washed once and then resuspended in 200 µl of PBS lysis buffer. Cell fractions were then combined with 4× Laemmli buffer loading dye and heated to 95 °C for 3 min. Samples were then separated by SDS–PAGE and cathepsin activity measured using a 488-nm laser on a Typhoon scanner (no. FLA 9500). The bottom sections of SDS–PAGE gels were subjected to Coomassie staining to visualize histones, followed by immunonblot transfer to a 0.45-µm polyvinylidene difluoride (PVDF) membrane (Millipore, Immobilin-P, no. IPVH00010). Infected whole-cell lysates for analysis by SDS–PAGE were generated

by washing cells three times in PBS at the indicated time points and then directly lysing them in 1× Laemmli buffer loading dye. Lysates were then heated to 95 °C for 3 min and analysed by immunoblot. Before SDS–PAGE, nuclear DNA was mechanically sheared using a Hamilton syringe.

To examine cathepsin B trafficking to the nucleus in the presence of the CA-074-Me inhibitor, RAW264.7 cells were infected with wild-type and heat-killed wild type (65 °C for 15 min) in a six-well format as described above. After cells were treated for 1 h with gentamicin, they were then incubated in the presence of absence of the indicated CA-074-Me concentrations or DMSO solvent control for the remainder of the experiment. Twenty hours later, cells were washed twice and lysed in 200 µl of PBS lysis buffer and allowed to lyse on ice for 10 min. Nuclei were then resuspended in 1× Laemmli buffer loading dye, sonicated in a bath sonicator and heated to 95 °C for 3 min. Samples were then separated by SDS–PAGE, and the bottom the gel was subjected to Coomassie staining to visualize histones. The resmainderof the gel was transferred to a PVDF membrane and probed as described below.

Membranes were blocked with 5% skim milk in Tris-buffered saline (TBS-T) overnight and probed with the following antibodies: RpoD, 1:1,000; GAPDH, 1:10,000; lamin A, 1:5,000; histone H3, 1:1,000; H3.cs1, 1:1,000; cathepsin B, 1:2,000; caspase-11, 1:1,000. Secondary antibodies were used at 1:5,000 and incubated with washed membranes for 1 h at room temperature. After washing, chemiluminescence substrate (GE Healthcare, no. RPN2106) was used for signal development and detected using X-ray film (Advantsta, no. L-07013-100) or a BioRad ChemoDoc Touch. X-ray film was converted to digital format by scanning at 300 × 300 dots per inch. Digital images were then cropped and contrast adjusted in Photoshop and incorporated into figures using Adobe Illustrator. Biological replicate samples were analysed on separate SDS–PAGE gels unless otherwise stated.

LDH release assay. RAW264.7 and iMACs were seeded in DMEM containing 10% FBS (DMEM + FBS) at a cell density of 3×10^4 per well in 96-well plates, and infected as described above with the following alterations. Unless otherwise stated, inhibitors and DMSO solvent were added at $t = 0$ h (see definition above). BMDMs were seeded in RPMI + FBS (5%) without phenol and supplemented with 40 ng ml^{-1} M-CSF at 5×10^4 cells per well into a 96-well plate (Thermo Fisher Scientific, catalogue no. 167008) ~18–20 h before infection. The bacterial inoculum was prepared as described above. To opsonize bacteria, pellets were resuspended in RPMI containing 10% mouse serum and incubated at room temperature for 20 min. Opsonized bacteria were added directly to wells containing BMDMs, iMACs or RAW264.7 cells at an MOI of 100:1 and centrifuged at 170*g* for 5 min to promote bacterial uptake. Infected cells were incubated at 37 °C under 5% CO_2 for 25 min. Cells were then washed once, media were replaced with RPMI + FBS (5%) without phenol, or DMEM + FBS (5%) without phenol for RAW264.7 and iMAC cells, containing 100 µg ml^{-1} gentamicin, and returned to the incubator for 1 h. Media were then replaced with RPMI + FBS (5%) (BMDMs) or DMEM + FBS (5%) (RAW264.7 and iMACs) without phenol and with 16 µg ml^{-1} gentamicin for the remainder of the experiment: this step denotes $t = 0$ h. LPS transfection of RAW264.7 cells was performed as previously described[19] using LPS (*E. coli* 0111:B4; Sigma, no. L2630), except that cells were seeded at 3×10^4 per well of a 96-well plate. LDH release as a measure of cell death was quantified by measuring percentage LDH release, as previously described, using the CytoTox 96 Non-Radioactive Cytotoxicity Assay kit (Promega, no. G1780)[17] according to the manufacturer's instructions. Percentage cell death = 100 × (experimental – spontaneous LDH)/(maximum LDH release – spontaneous LDH). Data were visualized in R and GraphPad Prism. Each experimental batch consisted of 3–8 (RAW264.7 and BMDMs) or 8–29 (iMACs) biological replicate wells per condition, whereby single measurements (490 nm) were acquired per well. Measurements were then normalized to spontaneous LDH release from uninfected wells that were otherwise identically treated, using the aforementioned formula and treated as a separate data point. Under our experimental conditions, the degree of overall LDH release during *S*Tm infection displayed considerable variance across batches of BMDM cells. To reduce this variance, batches in which wild-type *S*Tm induced <10% and >50% LDH release in RAW264.7 cells and BMDMs were removed (except for experiments where cells were infected with exponentially growing SPI-1 ON *S*Tm).

Microscopy. RAW264.7 cells were seeded in DMEM containing 10% FBS (DMEM + FBS) at a density of 4×10^5 cells per well in 24-well glass-bottom tissue culture plates (Greiner, no. 662892). Cells were infected with pDiGc-expressing bacteria as described above (MOI = 100:1). At the indicated times, cells were then treated with DCG04-Boclicky-TAMRA for 2 h before harvest. Cells were washed three times with PBS and then fixed in PBS solution containing 4% formaldehyde. Cells were then stained overnight with 2 µg ml^{-1} Hoechst 33342 and in PBS containing 0.05% Tx-100 to visualize host cell nuclei and host cytoskeleton, respectively. Images of stained cells were acquired on a Zeiss Cell Observer microscope using a ×20 objective. Images were processed using CellProfiler software v.2.1.1 as previously described[47]. Nuclear cathepsin activity was quantified by measuring the integrated DCG04-Boclicky-TAMRA signal intensity that overlapped with the host nucleus as defined by the Hoechst 33342 channel. Similarly, non-nuclear cathepsin activity was calculated by subtracting nuclear cathepsin activity from total cathepsin activity per cell. Cathepsin activity was then normalized to the nuclear size (area), and non-nuclear cathepsin activity was normalized to the total cell area of the cell minus the nuclear area.

Confocal images were acquired on an Olympus confocal laser scanning microscope (FV3000) using a ×60 oil-immersion objective. Samples were prepared as described above in a glass-bottomed 96-well plate. After three washes in PBS, cells were fixed with 4% formaldehyde and 0.4% Tx-100 in PBS for 1 h at room temperature. Images were captured using the 405-nm laser for excitation for Hoechst 33342, 488-nm for GFP-expressing (pDiGc) *S*Tm and 561-nm for DCG04-Boclicky-TAMRA. Image overlays and greyscale conversions were done in FIJI, then images were cropped in Photoshop before figure construction with Adobe Illustrator. Single planes from a z-stack are represented to provide a sharp boundary definition between the nucleus (Hoechst 33342 overlap) and non-nuclear cathepsin activity.

Bacterial growth curves. Overnight bacterial cultures grown at 37 °C in LB (Lennox) were pelleted at 8,000*g* and washed three times in fresh media, then back-diluted to $OD_{578} = 0.005$ in the presence of inhibitors and solvent at the indicated concentrations. Cells were dispensed, 100 µl per well, into a round-bottom 96-well plate in triplicate (Nunclon Delta Surface, Thermo Fisher Scientific, catalogue no. 168136), then covered with a sealable transparent breathable membrane (Breathe-Easy, Divbio, catalogue no. BEM-1). Cell growth was quantified by measuring absorbance at 578 nm at 20-min intervals with constant shaking at 37 °C.

Generation of stefin B-expressing iMACs. Immortalized wild-type iMACs and their retroviral transduction thereof were previously described[48], and HEK cells were cultured in DMEM containing 10% heat-inactivated FCS, 100 U ml^{-1} penicillin/streptomycin and 2 mM GlutaMAX. iMACs were routinely tested for *Mycoplasma* using a direct growth assay on conditioned media. Immortalized wild-type iMACs were retrovirally transduced with either the listed stefin B constructs or a control construct containing mCitrine only. Following transduction, the cells were sorted for comparable expression of both constructs at either high or low expression of mCitrine, by flow cytometry.

iMAC sample preparation and immunoblot. Samples for analysis of stefin B-expressing iMACs were prepared and immunoblot performed as described previously[49]. Briefly, cells were harvested, washed once in PBS and then lysed in RIPA lysis buffer (cOmplete protease inhibitors, Roche), then sonicated to disrupt DNA and thereby facilitate gel loading. The samples were then denatured and reduced by the addition of NuPAGE sample buffer (25% sample volume, Life technologies) and NuPAGE sample reducing agent (10% sample volume, Life technologies) and heating to 95 °C for 5 min. Proteins were separated by electrophoresis using a precast 4–12% SDS–PAGE gel (Novex, Invitrogen) and MES buffer (Novex, Invitrogen). The proteins were transferred to an Immobilon-FL PVDF membrane (Millipore) and blocked using 3% BSA in Tris-buffered saline pH 7.4 (BSA-TBS) for 1 h. The membrane was then probed with an anti-Flag antibody (Clone M2, Sigma) at 1:1,000 dilution and an anti-tubulin antibody (CST) at 1:1,000 dilution in BSA-TBS with 0.1% Tween overnight at 4 °C. Secondary antibodies (coupled to IRDye 680RD ot IRDye 800CW, Li-Cor Biosciences) were used at 1:25,000 dilution.

Immunofluorescence of iMAC cells. Cells were fixed in 4% paraformaldehyde (Sigma) for 20 min, washed five times in PBS then permeabilized by incubation with 0.3% Triton X-100 diluted in PBS for 5 min. Cells were then incubated in immunofluorescence staining solution (PBS containing 1% heat-inactivated FCS, 10% goat serum) for 1 h at ambient temperature to block non-specific antibody binding. Primary antibody (anti-Flag 1:1,000, Clone M2, Sigma)) diluted in immunofluorescence staining solution was added to the cells followed by overnight incubation at 4 °C. Cells were washed three timres in staining solution then incubated with Alexa 647 conjugated mouse IgG antibody (1:800 dilution in staining solution, Life Technologies) at room temperature for 1 h. Cells were then washed three times, incubated with DAPI for 5 min to visualize nucleic acid (1 ug ml^{-1}, Life Technologies) and washed once. Cells were imaged using an Observer.ZI epifluorescence microscope, ×20 objective (dry, PlanApochromat, numerical aperture 0.8; Zeiss), Axiocam 506 mono and ZEN blue software.

iMAC stimulation conditions. Stefin B-expressing and control iMACs were harvested and plated at 0.8×10^4 cells per well in a 96-well plate and left to adhere for 3 h. To assess LDH release after activation of the NLRP3 inflammasome, cells were washed once and primed with 200 ng ml^{-1} Ultra-pure LPS (Invivogen, tlrl-3pelps) for 3 h in DMEM containing 1% heat-inactivated FCS. Next, 10 µM nigericin (Invitrogen, no. N1495) was added and the cells incubated for a further 1.5 h. To assess LDH release following the addition of Leu-Leu-o-Methyl ester (LLoMe; Santa Cruz, no. 16889-14-8), cells were washed once and treated with 1 mM LLoMe for 2 h in DMEM containing 1% heat-inactivated FCS. For both assays the 96-well plate was centrifuged at 400*g* for 5 min, supernatants were then harvested and LDH release was measured from the supernatant using the LDH cytotoxicity kit (Pierce, no. 10008882).

2D-TPP. Two-dimensional thermal proteome profiling was performed as previously described[21]. Briefly, RAW264.7 macrophages were infected with overnight cultures of wild-type *S*Tm as described above, and CA-074-Me was added to final concentrations of 1, 4, 20 and 100 µM as well as a DMSO control, together with 16 µg ml^{-1} gentamicin. Two wells of a six-well plate were pooled for each condition (that is, ~1.8 × 10^6 cells per condition times five conditions). Drug treatment was retained throughout the infection. After 20 h, cells were washed twice with PBS, aliquoted to a PCR plate and heated for 3 min to ten different temperatures (37–67 °C) in a PCR machine (Agilent SureCycler 8800). Lysis buffer (final concentration, 0.8% NP40, 1.5 mM $MgCl_2$, 1× protease inhibitor (Roche), 1× phosphatase inhibitor (Roche) and 250 U ml^{-1} benzonase in PBS) was added and cells were lysed for 1 h at 4 °C. Protein aggregates were then removed as previously described[50], and the remaining soluble proteins were digested according to a modified SP3 protocol[51,52]. Peptides were labelled with TMT10plex (Thermo Fisher Scientific), fractionated into 12 fractions under high-pH conditions and analysed by LS–MS/MS, as previously described[50]. Protein identification and quantification was performed using IsobarQuant[53] and Mascot 2.4 (Matrix Science) against a concatenated FASTA file with *S.* Typhimurium (Proteome ID: UP000001014) and *Mus musculus* (Proteome ID: UP000000589) proteins. Data were analysed with the *TPP* package for R[53].

Caspase-11 activity assay. Caspase-11 activity was measured as previously described[54]. In brief, 10 U 100 µl^{-1} recombinant caspase-11 (mouse, Enzo life sciences, no. BML-SE155-5000) in caspase activity buffer (200 mM NaCl, 50 mM HEPES pH 8.0, 50 mM KCl, 10 mM DTT) supplemented with 100 µM AcLEHD-afc (Santa Cruz, no. sc-311277) was incubated in the presence of CA-074-Me, E64d (Sigma, no. E8640) and the caspase-9/11 inhibitor Z-LEHD-FMK (Abcam, no. ab142026) or a DMSO solvent control at the concentrations indicated in the figure legends. Hydrolysis of the caspase-11 substrate was measured at regular time intervals at 37 °C using an Infinite M1000Pro TECAN spectroflourometer in a 96-well flat-bottom transparent plate (Thermo Fisher Scientific, no. 167008) (excitation 400 nm, emission 505 nm).

Statistical analyses. For cell death (LDH release) assays, significance testing was performed in R using the unpaired *t*-test (Figs. 5b,d,e and 6c,e). To avoid assumption of any shape of the distribution for single-cell nucleus analysis of cathepsin activity, statistical testing was performed in R using the unpaired Wilcoxon rank-sum test (non-parametric) (Fig. 4d). For proteomics data, statistical tests were performed using the Limma package in R/Bioconductor as previously described[8]. Briefly, after fitting a linear model to the data, an empirical Bayes moderated *t*-test was used and *P* values were adjusted for multiple testing with the Benjamini–Hochberg method. Gene Ontology (GO) enrichment was calculated with the ClueGO plugin v.2.1.7 of Cytoscape v.3.3.0. For the global analyses described (Fig. 1b), GO enrichment was performed on proteins displaying ±1.5 $\log_2$(fold-change) (infected/uninfected). For comparison between *S*Tm- and LPS-stimulated cells (Fig. 2a,b), GO enrichment was performed on proteins ±2 s.d. of $\log_2$(fold-change) (infected/uninfected). A custom reference set was used for each test, and contained all quantified proteins within the same fraction. GO enrichment was performed separately on up- and downregulated proteins using the right-sided hypergeometric test, and corrected for multiple testing using the Bonferroni step-down (Holm) method. This test was chosen for stringent error control.

Reporting Summary. Further information on research design is available in the Nature Research Reporting Summary linked to this article.

Data availability

Proteomic pSILAC-AHA data have been deposited at ProteomeXchange (http://www.proteomexchange.org/) under the identifiers PXD010179 (pSILAC-AHA) and PXD016086 (2D-TPP). Source data for Figs. 1–6 and Extended Data Figs. 1–7 and 10 are provided with the paper.

Code availability

The code and pipelines used for data analysis are available upon request.

Received: 8 November 2018; Accepted: 6 May 2020;
Published online: 8 June 2020

References

1. Broz, P. & Dixit, V. M. Inflammasomes: mechanism of assembly, regulation and signalling. *Nat. Rev. Immunol.* **16**, 407–420 (2016).
2. Shi, J. et al. Inflammatory caspases are innate immune receptors for intracellular LPS. *Nature* **514**, 187–192 (2014).
3. Kayagaki, N. et al. Caspase-11 cleaves gasdermin D for non-canonical inflammasome signalling. *Nature* **526**, 666–671 (2015).
4. Shi, J. et al. Cleavage of GSDMD by inflammatory caspases determines pyroptotic cell death. *Nature* **526**, 660–665 (2015).
5. Aachoui, Y. et al. Caspase-11 protects against bacteria that escape the vacuole. *Science* **339**, 975–978 (2013).
6. Eichelbaum, K., Winter, M., Berriel Diaz, M., Herzig, S. & Krijgsveld, J. Selective enrichment of newly synthesized proteins for quantitative secretome analysis. *Nat. Biotechnol.* **30**, 984–990 (2012).
7. Figueira, R., Watson, K. G., Holden, D. W. & Helaine, S. Identification of *Salmonella* pathogenicity island-2 type III secretion system effectors involved in intramacrophage replication of *S. enterica* serovar Typhimurium: implications for rational vaccine design. *mBio* **4**, e00065 (2013).
8. Eichelbaum, K. & Krijgsveld, J. Rapid temporal dynamics of transcription, protein synthesis, and secretion during macrophage activation. *Mol. Cell. Proteomics* **13**, 792–810 (2014).
9. McGourty, K. et al. *Salmonella* inhibits retrograde trafficking of mannose-6-phosphate receptors and lysosome function. *Science* **338**, 963–967 (2012).
10. Goulet, B. et al. A cathepsin L isoform that is devoid of a signal peptide localizes to the nucleus in S phase and processes the CDP/Cux transcription factor. *Mol. Cell* **14**, 207–219 (2004).
11. Tamhane, T. et al. Nuclear cathepsin L activity is required for cell cycle progression of colorectal carcinoma cells. *Biochimie* **122**, 208–218 (2016).
12. Goulet, B. et al. Increased expression and activity of nuclear cathepsin L in cancer cells suggests a novel mechanism of cell transformation. *Mol. Cancer Res.* **5**, 899–907 (2007).
13. Konjar, S., Yin, F., Bogyo, M., Turk, B. & Kopitar-Jerala, N. Increased nucleolar localization of SpiA3G in classically but not alternatively activated macrophages. *FEBS Lett.* **584**, 2201–2206 (2010).
14. Turk, V. et al. Cysteine cathepsins: from structure, function and regulation to new frontiers. *Biochim. Biophys. Acta* **1824**, 68–88 (2012).
15. Tedelind, S. et al. Nuclear cysteine cathepsin variants in thyroid carcinoma cells. *Biol. Chem.* **391**, 923–935 (2010).
16. Duncan, E. M. et al. Cathepsin L proteolytically processes histone H3 during mouse embryonic stem cell differentiation. *Cell* **135**, 284–294 (2008).
17. Brennan, M. A. & Cookson, B. T. *Salmonella* induces macrophage death by caspase-1-dependent necrosis. *Mol. Microbiol.* **38**, 31–40 (2000).
18. Fink, S. L. & Cookson, B. T. Caspase-1-dependent pore formation during pyroptosis leads to osmotic lysis of infected host macrophages. *Cell. Microbiol.* **8**, 1812–1825 (2006).
19. Napier, B. A. et al. Complement pathway amplifies caspase-11-dependent cell death and endotoxin-induced sepsis severity. *J. Exp. Med* **213**, 2365–2382 (2016).
20. Savitski, M. M. et al. Tracking cancer drugs in living cells by thermal profiling of the proteome. *Science* **346**, 1255784 (2014).
21. Becher, I. et al. Thermal profiling reveals phenylalanine hydroxylase as an off-target of panobinostat. *Nat. Chem. Biol.* **12**, 908–910 (2016).
22. Hentze, H., Lin, X. Y., Choi, M. S. K. & Porter, A. G. Critical role for cathepsin B in mediating caspase-1-dependent interleukin-18 maturation and caspase-1-independent necrosis triggered by the microbial toxin nigericin. *Cell Death Differ.* **10**, 956–968 (2003).
23. Pelegrin, P., Barroso-Gutierrez, C. & Surprenant, A. P2X7 receptor differentially couples to distinct release pathways for IL-1beta in mouse macrophage. *J. Immunol.* **180**, 7147–7157 (2008).
24. van der Velden, A. W., Lindgren, S. W., Worley, M. J. & Heffron, F. *Salmonella* pathogenicity island 1-independent induction of apoptosis in infected macrophages by *Salmonella enterica* serotype Typhimurium. *Infect. Immun.* **68**, 5702–5709 (2000).
25. Broz, P. et al. Caspase-11 increases susceptibility to *Salmonella* infection in the absence of caspase-1. *Nature* **490**, 288–291 (2012).
26. Monack, D. M., Detweiler, C. S. & Falkow, S. *Salmonella* pathogenicity island 2-dependent macrophage death is mediated in part by the host cysteine protease caspase-1. *Cell. Microbiol.* **3**, 825–837 (2001).
27. Shi, L. et al. Proteomic investigation of the time course responses of RAW 264.7 macrophages to infection with *Salmonella enterica*. *Infect. Immun.* **77**, 3227–3233 (2009).
28. Hui, W. W. et al. *Salmonella enterica* serovar Typhimurium alters the extracellular proteome of macrophages and leads to the production of proinflammatory exosomes. *Infect. Immun.* **86**, e00386-17 (2018).
29. Roberts, L. R. et al. Cathepsin B contributes to bile salt-induced apoptosis of rat hepatocytes. *Gastroenterology* **113**, 1714–1726 (1997).
30. Vancompernolle, K. et al. Atractyloside-induced release of cathepsin B, a protease with caspase-processing activity. *FEBS Lett.* **438**, 150–158 (1998).
31. Maher, K. et al. A role for stefin B (cystatin B) in inflammation and endotoxemia. *J. Biol. Chem.* **289**, 31736–31750 (2014).
32. Mateus, A., Määttä, T. A. & Savitski, M. M. Thermal proteome profiling: unbiased assessment of protein state through heat-induced stability changes. *Proteome Sci.* **15**, 13 (2016).
33. Szklarczyk, D. et al. The STRING database in 2017: quality-controlled protein-protein association networks, made broadly accessible. *Nucleic Acids Res.* **45**, D362–D368 (2017).
34. Greenbaum, D. et al. Chemical approaches for functionally probing the proteome. *Mol. Cell. Proteom.* **1**, 60–68 (2002).

35. Turk, B., Turk, D. & Salvesen, G. S. Regulating cysteine protease activity: essential role of protease inhibitors as guardians and regulators. *Curr. Pharm. Des.* **8**, 1623–1637 (2002).
36. Orlowski, G. M. et al. Multiple cathepsins promote pro-IL-1β synthesis and NLRP3-mediated IL-1β activation. *J. Immunol.* **195**, 1685–1697 (2015).
37. Porwollik, S. et al. Defined single-gene and multi-gene deletion mutant collections in *Salmonella enterica* sv Typhimurium. *PLoS ONE* **9**, e99820 (2014).
38. Helaine, S. et al. Dynamics of intracellular bacterial replication at the single cell level. *Proc. Natl Acad. Sci. USA* **107**, 3746–3751 (2010).
39. Li, P. et al. Mice deficient in IL-1 beta-converting enzyme are defective in production of mature IL-1 beta and resistant to endotoxic shock. *Cell* **80**, 401–411 (1995).
40. Kayagaki, N. et al. Non-canonical inflammasome activation targets caspase-11. *Nature* **479**, 117–121 (2011).
41. Martinon, F., Pétrilli, V., Mayor, A., Tardivel, A. & Tschopp, J. Gout-associated uric acid crystals activate the NALP3 inflammasome. *Nature* **440**, 237–241 (2006).
42. Mariathasan, S. et al. Differential activation of the inflammasome by caspase-1 adaptors ASC and Ipaf. *Nature* **430**, 213–218 (2004).
43. Beuzón, C. R. et al. *Salmonella* maintains the integrity of its intracellular vacuole through the action of SifA. *EMBO J.* **19**, 3235–3249 (2000).
44. Yang, F., Shen, Y., Camp, D. G. II & Smith, R. D. High-pH reversed-phase chromatography with fraction concatenation for 2D proteomic analysis. *Expert Rev. Proteomics* **9**, 129–134 (2012).
45. Vizcaíno, J. A. et al. The PRoteomics IDEntifications (PRIDE) database and associated tools: status in 2013. *Nucleic Acids Res.* **41**, D1063–1069 (2013).
46. Babicki, S. et al. Heatmapper: web-enabled heat mapping for all. *Nucleic Acids Res.* **44**, W147–153 (2016).
47. Ochoa, D. et al. An atlas of human kinase regulation. *Mol. Syst. Biol.* **12**, 888 (2016).
48. Hornung, V. et al. Silica crystals and aluminum salts activate the NALP3 inflammasome through phagosomal destabilization. *Nat. Immunol.* **9**, 847–856 (2008).
49. Stutz, A. et al. NLRP3 inflammasome assembly is regulated by phosphorylation of the pyrin domain. *J. Exp. Med.* **214**, 1725–1736 (2017).
50. Mateus, A. et al. Thermal proteome profiling in bacteria: probing protein state in vivo. *Mol. Syst. Biol.* **14**, e8242 (2018).
51. Hughes, C. S. et al. Single-pot, solid-phase-enhanced sample preparation for proteomics experiments. *Nat. Protoc.* **14**, 68–85 (2019).
52. Hughes, C. S. et al. Ultrasensitive proteome analysis using paramagnetic bead technology. *Mol. Syst. Biol.* **10**, 757 (2014).
53. Franken, H. et al. Thermal proteome profiling for unbiased identification of direct and indirect drug targets using multiplexed quantitative mass spectrometry. *Nat. Protoc.* **10**, 1567–1593 (2015).
54. Ross, C., Chan, A. H., Von Pein, J., Boucher, D. & Schroder, K. Dimerization and auto-processing induce caspase-11 protease activation within the non-canonical inflammasome. *Life Sci. Alliance* **1**, e201800237 (2018).

Acknowledgements

We thank the EMBL Flow Cytometry, Proteomics and ALMF Core Facilities; N. Kurzawa for 2D-TPP data analysis; S. Helaine (Imperial College) for the pDiGc plasmid; O. Wagih (EBI) for R scripts; K.-M. Noh (EMBL) for the H3.cs1 antibody; and members of the Typas and Krijgsveld laboratories for discussions. We acknowledge funding from EMBL for this research. J.S., N.L. and H.I. were supported by Marie Skłodowska-Curie Actions COFUND grant no. 291772, and A.M. by grant no. 664726. E.L. was supported by the Deutsche Forschungsgemeinschaft (German Research Foundation) under Germany's Excellence Strategy (nos. EXC2151 and 390873048) and the ERC consolidator grant InflammAct. N.L. is now supported by the National Key Research and Development Programme of China (no. 2018YFA0902703), the Shenzhen Science and Technology Innovation Committee (no. JCYJ20170818164014753) and the National Natural Science Foundation of China (nos. 31800694 and 31971354). N.K.-J. and B.T. were supported by the Slovene Research Agency (no. P1-0140).

Author contributions

Conceptualization was carried out by J.S., J.K. and A.T. Investigation was done by J.S., N.L., A.M., G.S., M.S. and J.K. (proteomics), and by J.S., J.B., A.S., M.S., J.M. and M.Z. (molecular biology, biochemistry and cell biology). Resources were provided by B.I.F., H.S.O. (cathepsin reactive probes), M.M., E.L. (iMACs), N.K.-J., B.T. (stefin B construct), A.H. and W.-D.H. (BMDMs). Data analysis was performed by J.S., M.M., A.S., B.E.D., N.L., H.I. and A.M. The article was written by J.S. and A.T. with input from all authors. The figures were made by J.S., except for 2D-TPP (A.M.), bacterial growth curves (A.S.) and iMAC data (M.M.), with input from J.K. and A.T. The study was supervised by A.T., J.K., M.S., E.L. and P.B. Funding acquisition was carried out by A.T. and J.K.

Competing interests

The authors declare no competing interests.

Additional information

Extended data is available for this paper at https://doi.org/10.1038/s41564-020-0736-7.

Supplementary information is available for this paper at https://doi.org/10.1038/s41564-020-0736-7.

Correspondence and requests for materials should be addressed to J.K. or A.T.

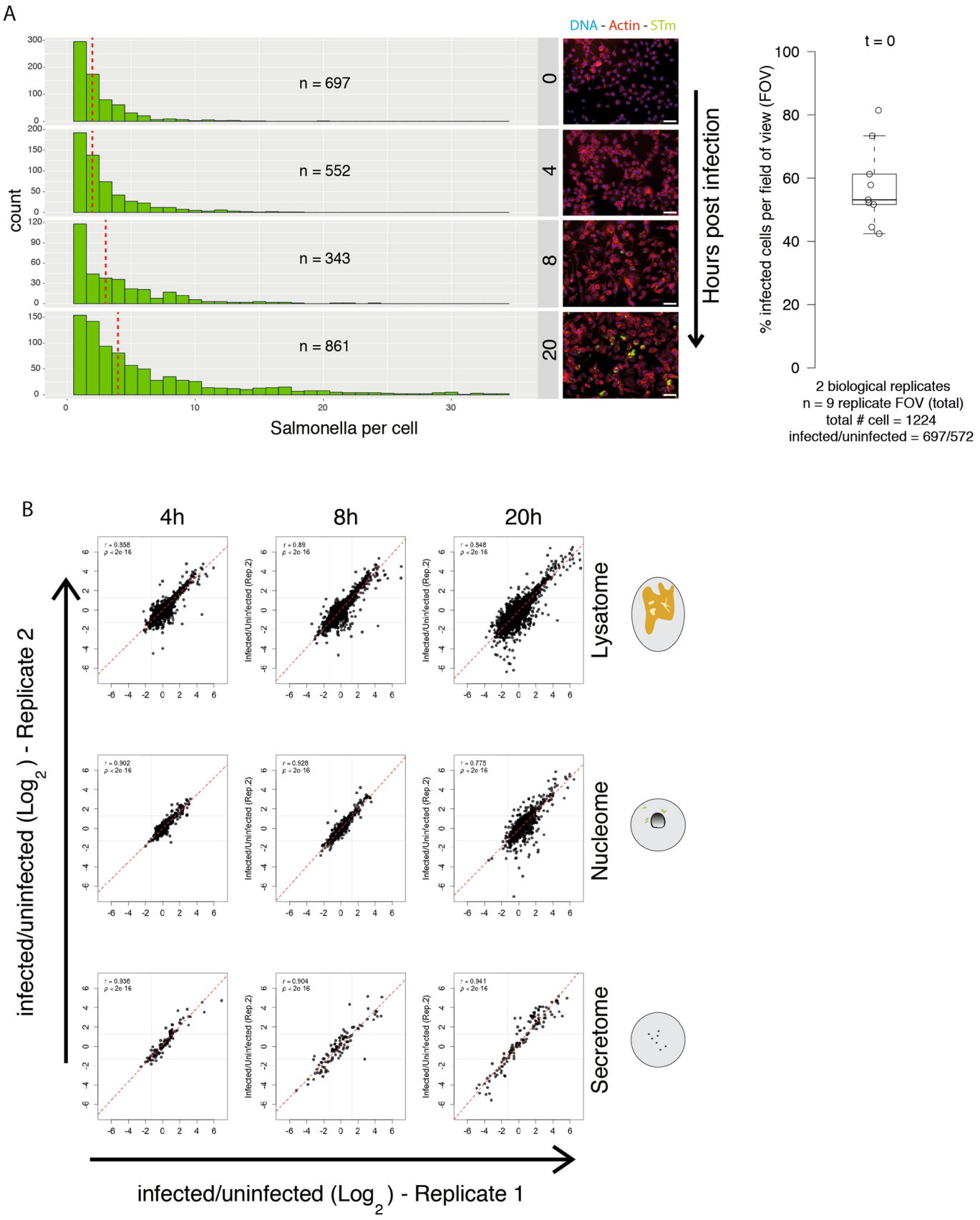

Extended Data Fig. 1 | See next page for caption.

Extended Data Fig. 1 | Increasing intracellular STm load over time co-occurs with dynamic proteome changes. a) RAW264.7 cells infected with *STm* constitutively expressing mCherry (pFCcGi) at MOI 100:1 and incubated for the indicated times were analysed by CellProfiler. SPI-1 OFF bacteria were chosen to mimic the pathogen-host interaction at systemic sites. After bacterial internalization, cells were treated with gentamicin to kill non-internalised bacteria, synchronise the infection and avoid re-infection cycles. The intracellular bacterial load was quantified at the single-cell level to ensure sampling times spanned distinct phases of intracellular *STm* proliferation states i.e. pre-proliferation (4h), initial (8h) and extensive (20h) proliferation post uptake. Images were captured at 20x objective and analysis was conducted with CellProfiler to segment infected from uninfected cells and quantify bacterial load per cell based on mCherry fluorescence per infected cell. CellProfiler quantification of bacterial count per infected cell (only infected cells) are displayed as a histogram and shows increasing bacterial load with time. Data contains combined counts from two biological replicate experiments, whereby each replicate received reverse SILAC labels (see Methods). 2-5 fields of view (technical replicates) were acquired per biological replicate and per time point. The combined total of infected host cells quantified is indicated (n=). The dotted red line indicates distribution median. Representative images of quantified cells are displayed to the right of histograms. Scale bars represent 50 μm. The % of infected cells per field of view (FOV) at the beginning of the experiment (i.e. immediately post gentamicin 100 μg/ml treatment, *t*=0) is displayed as a boxplot on the far right. Box plots are depicted as in Fig. 3C. n denotes FOV, amounting to 1224 cells in total (infected & non-infected). b) Replicate correlation of infected versus uninfected samples for the indicated time points and different subcellular fractions - cytoplasmic and solubilised organelles within the Tx-100 soluble fraction (lysatome; upper), nuclear enriched fraction in the Tx-100 insoluble fraction (nucleome-middle) and proteins secreted into the culture supernatant (secretome-lower). Two biological replicates containing reversed SILAC labels were obtained for each cell fraction and each time point (See Supplementary Table 1). We observed concordant biological replicate correlation (r = Pearson's correlation) across all time points, and within each subcellular fraction (mean $r = 0.886$). Data is from n=2 biologically independent samples. A red dotted line represents a linear model by robust regression and r refers to the Pearson's correlation coefficient.

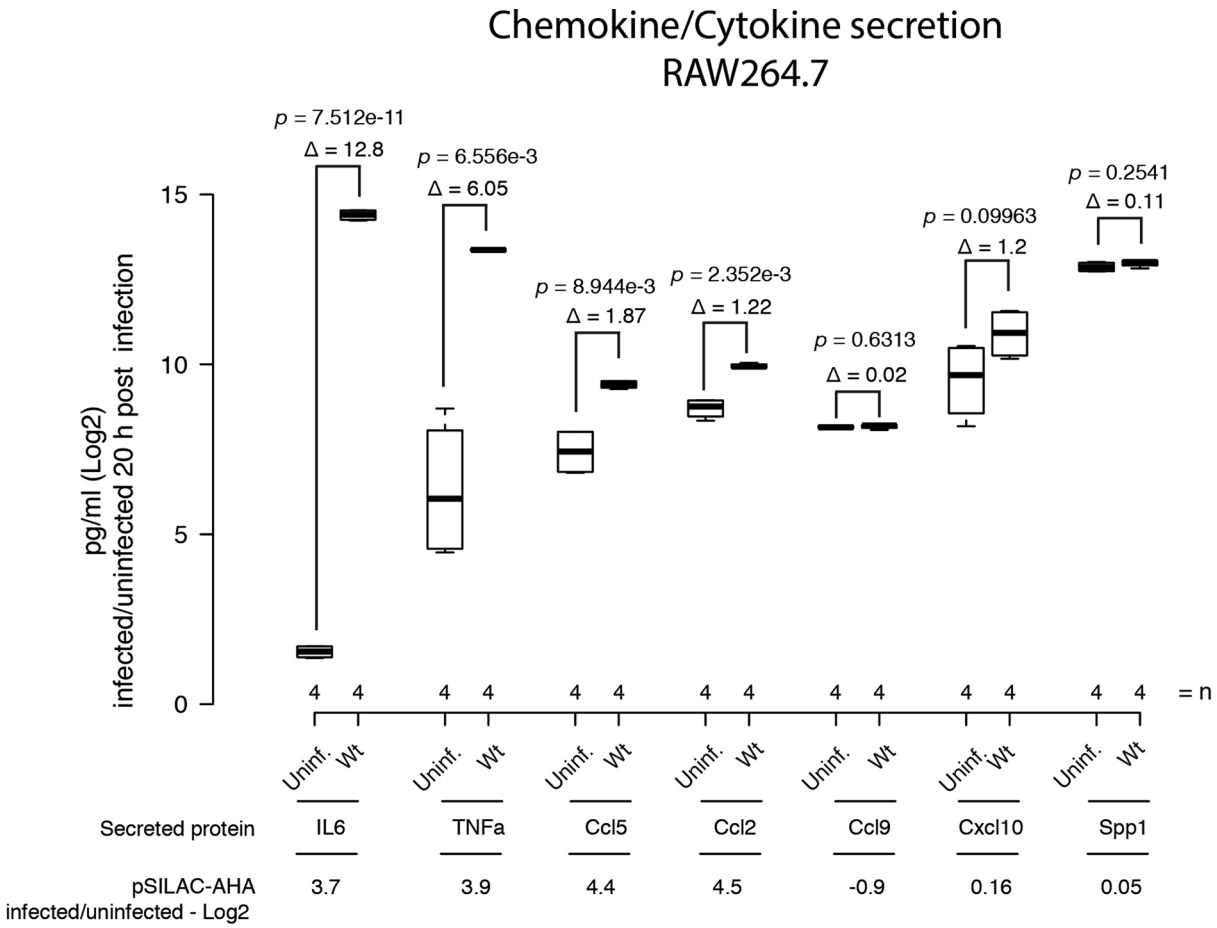

Extended Data Fig. 2 | Quantification of cytokine and chemokine release from RAW264.7 cells during STm infection. After RAW264.7 cells were infected with STm for 20 hours, the conditioned media was removed and indicated cytokines and chemokines were quantified using a custom array (Biocat, GmbH). n denotes the combined data from 2 independent experiments (batches), each batch containing 2 biological replicates per condition. Box boundaries indicate the upper and lower IQR, the median is depicted by the middle boundary and whiskers represent 1.5x IQR. Relative infected/uninfected Δ (Log_2) from the cytokine array are depicted within the plot for each protein. Corresponding pSILAC-AHA infected/uninfected (Log_2) ratios are presented below the corresponding protein for the 20hr post-infection time-point (with the exception of TNFa, which we could only detect at 8 hpi). Non-hits and hits match perfectly between the 2 methods. Fold effect differences between pSILAC-AHA and array-based quantification are most likely due to the fact that the cytokine assay measures steady-state protein levels and pSILAC-AHA newly synthesized proteins. As expected, for more abundant proteins, measuring steady-state levels masks changes in expression dynamics. A two-sided unpaired t-test was used to calculate *p*..

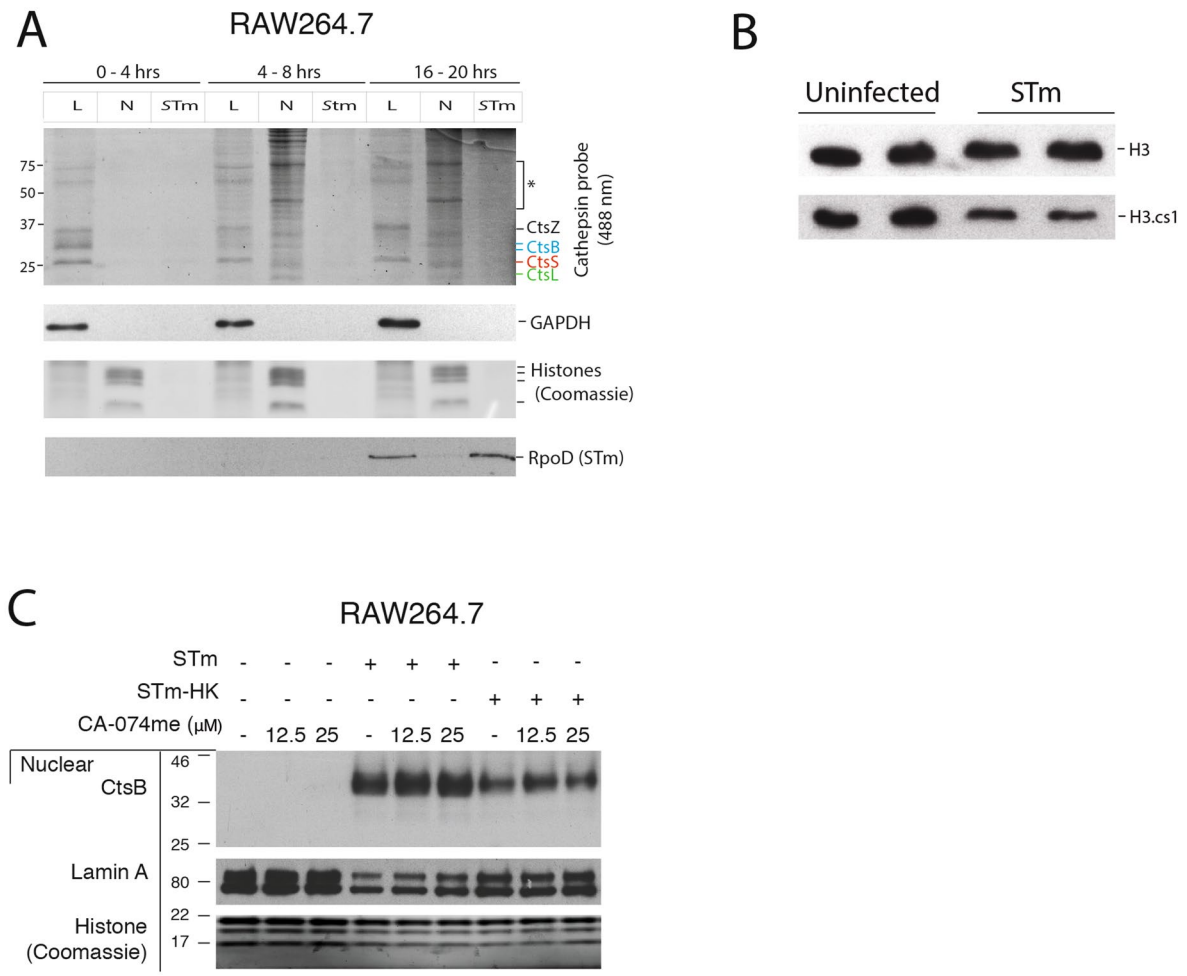

Extended Data Fig. 3 | Nuclear cathepsin translocation occurs already from 8 hpi, is independent of cathepsin activity and does not result in increased Histone 3 cleavage. a) Time course of nuclear cathepsin activity. Nuclei and *S*Tm were enriched by sequential 50 x *g* and 8,000 x *g* centrifugation steps, respectively. RAW264.7 cells were infected with wildtype *S*Tm 14028s and treated with DCG04-Bodipy-FLike (5μM) for 4 hours prior to harvesting. Samples were separated by SDS-PAGE and visualised using a fluorescent scanner (Excitation 405 nm/Emission 520 nm), followed by immunoblotting for the soluble cytoplasmic protein GAPDH, the bacterial protein RpoD and Coomassie staining for histones as a loading control for nuclear extracts. L = lysatome, N = nucleome, *S*Tm = *S*Tm enriched fraction. Experiment was performed once. b) RAW264.7 cells were infected with wildtype *S*Tm at MOI 100:1 and harvested at 20 hpi. Whole cell lysates were immunoblotted with the CtsL specific cleavage product of H3 (H3.cs1)[16] and histone 3 (H3) as loading control. The experiment was performed in biological duplicate per condition and were analysed in adjacent lanes. c) Nuclear extracts from RAW264.7 cells either mock infected, infected with wildtype *S*Tm or heat killed wildtype (*S*Tm-HK) for 20 hours. CA-074-Me was present throughout the infection experiment at the indicated concentrations. Nuclear extracts were analysed by immunoblot for CtsB (1:2,000), Lamin A (1:5,000) and histones by Coommassie stain (see Supplementary Information (SI) for second replicate data).

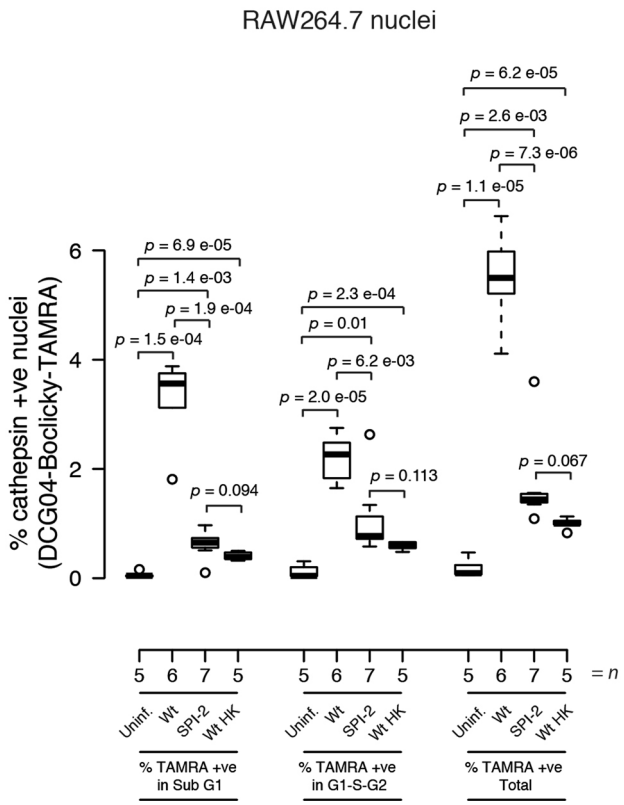

Extended Data Fig. 4 | Nuclear cathepsin activity is enhanced by wildtype STm and mildly by an ssaV mutant and heat killed bacteria. Nuclei were extracted from RAW264.7 cells treated with DCG04-Boclicky-TAMRA (5 μM) for 2 hours prior to harvest at 20 hpi with wildtype (Wt), a SPI-2 mutant (Δ*ssaV*) or heat killed wildtype bacteria (Wt HK) (MOI = 100:1). Samples were processed as described in Fig. 5a. Data is combined from two independent experiments (batches). n denotes the number of biologically independent samples. A two-sided unpaired t-test was used to calculate *p*. Boxplots are depicted as in Fig. 3C.

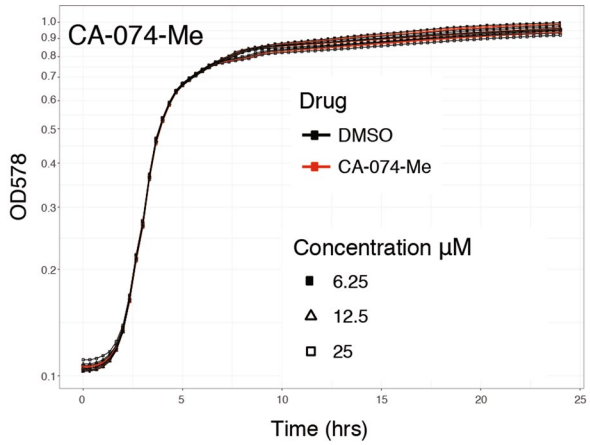

Extended Data Fig. 5 | STm growth is unaffected by the cathepsin inhibitor CA-074-Me in batch culture conditions. STm 14028s growth was measured in the presence of the selective cathepsin inhibitor CA-074-Me in LB 6, 12.5 and 25 µM and DMSO solvent controls. Drug concentrations used are indicated. Experiment was performed in biological triplicate.

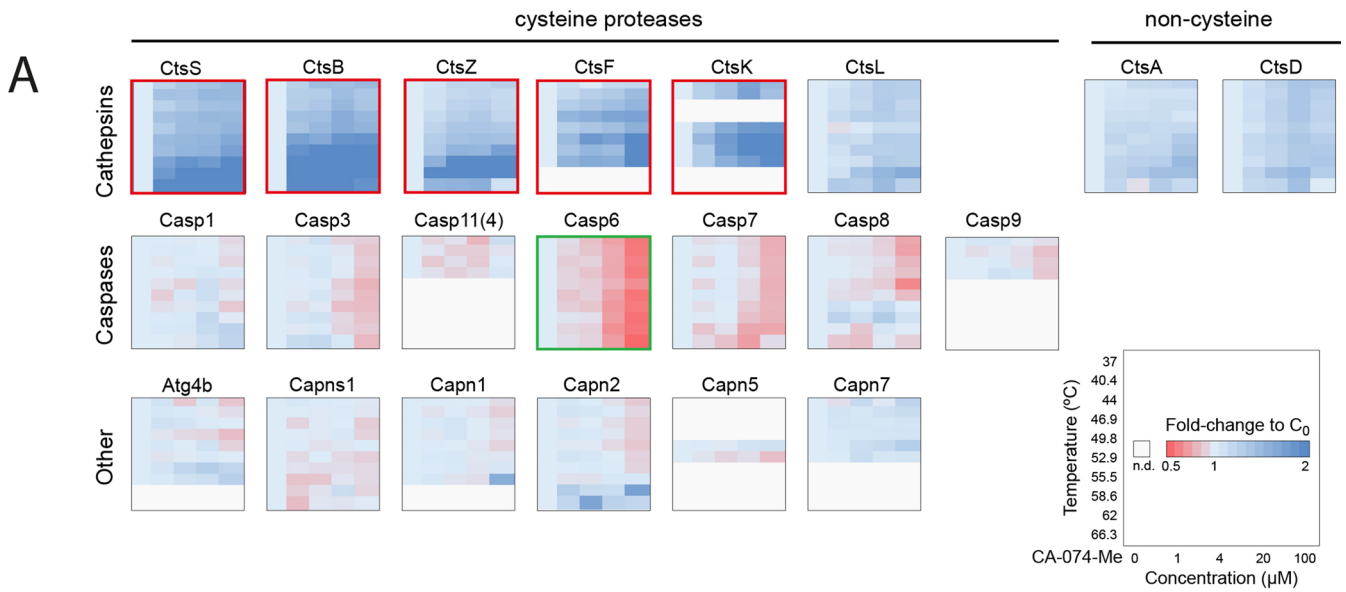

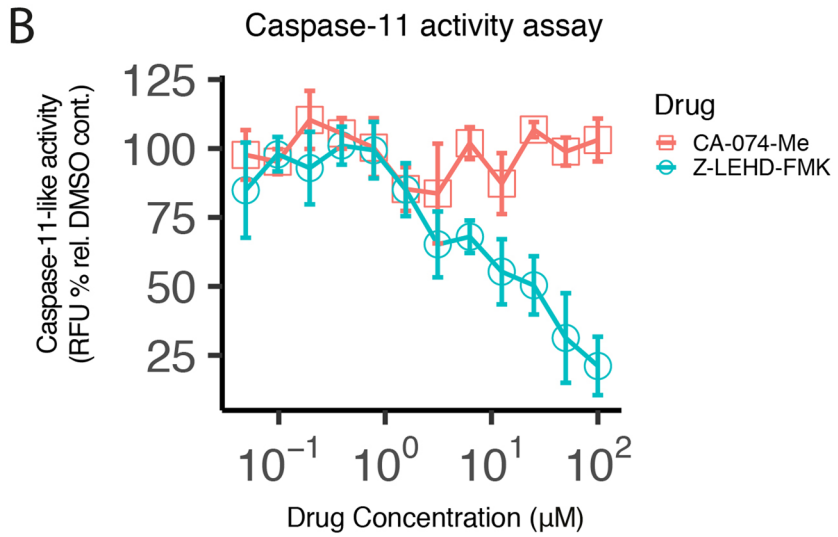

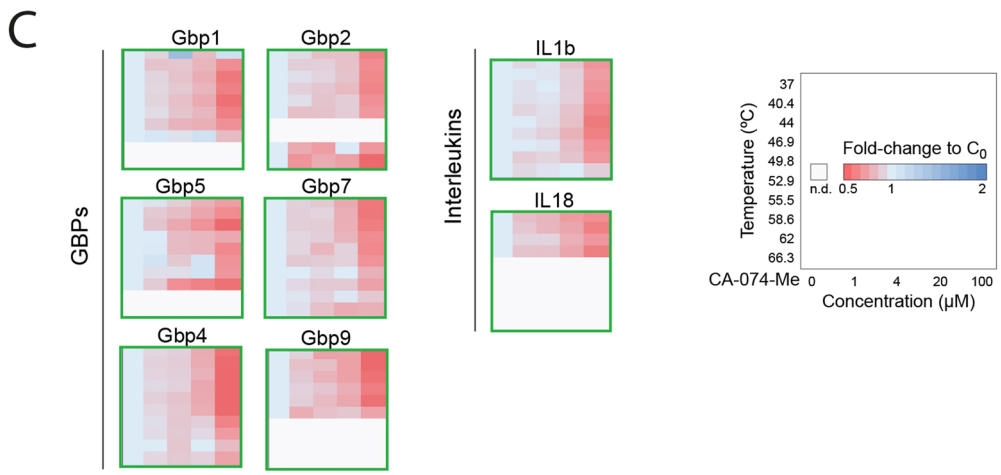

Extended Data Fig. 6 | See next page for caption.

Extended Data Fig. 6 | CA-074-Me inhibits cathepsins and reduces expression of proinflammatory proteins. a) 2D-TPP of RAW264.7 cells infected with wildtype *S*Tm 14028s for 20 hours in the presence of increasing concentrations of CA-074-Me (1-100 μM). To assess CA-074-Me specificity, we applied 2-dimensional Thermal Proteome Profiling (2D-TPP). 2D-TPP enables proteome assessment of protein ligand binding based on the principle that ligand-bound proteins are more thermally stable than proteins not bound to a ligand[20,21], and in parallel provides information of proteome-wide protein abundance. We subjected RAW264.7 cells infected with wildtype *S*Tm to increasing doses of CA-074-Me and compared proteome-wide thermostabilisation relative to solvent controlled cells (see methods). Increased (blue) or decreased fold changes are calculated by normalising the abundance of each protein relative to the abundance in the DMSO vehicle per temperature. Protein stabilization (red framed) is demonstrated by increasing (blue) fold changes with respect to increasing temperature (top to bottom) as well as with increasing drug concentrations (left to right). Changes in protein expression (green framed) can be detected if abundance changes are already evident from low temperatures i.e. before proteins melt. All cathepsins detected by 2D-TPP are displayed. CtsA and CtsD are serine and aspartic-acid proteases, respectively, and are therefore not targeted by CA-074-Me and serve as negative controls. Contrary to evidence demonstrating CA-074-Me targets CtsL[35], we failed to detect its stabilisation in our experiment. Cathepsins are arranged in the top row, followed by caspases and other cellular proteases in descending order. Note Caspase-1 stability was not affected by CA-074-Me, in line with previous reports[22]. Additionally, CA-074-Me reduced IL-1b expression as previously shown[35,36]. 2D-TPP data can be found in Supplementary Table 6. b) Caspase-11-like proteolysis activity was assessed using purified active Caspase-11 and measuring cleavage of the fluorescent substrate AcLEHD-afc as previously described[37]. Caspase-11-like proteolytic activity was assessed in the presence of indicated concentrations of CA-074-Me and the Caspase-11 inhibitor Z-LEHD-FMK as a positive control. Activity is expressed as the % of AcLEHD-afc cleavage relative to the DMSO solvent control. Data is combined from n = 3 biologically independent experiments; error bars depict standard deviation and the center value denotes the mean. c) 2D-TPP profiles of inflammation related proteins reduced in abundance upon CA-074-Me treatment. Data presented as in (a).

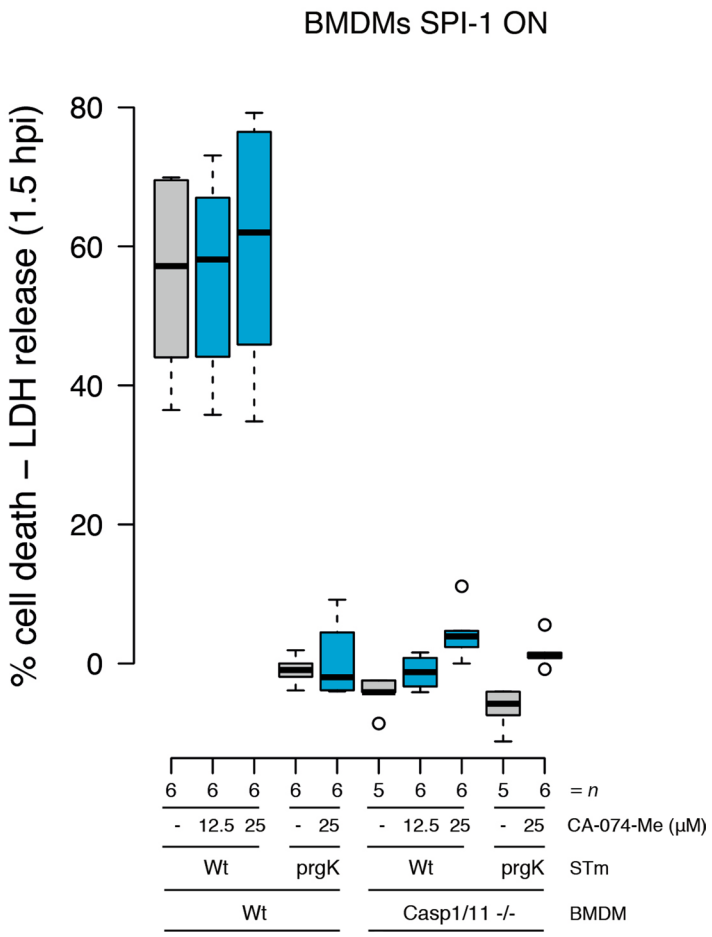

Extended Data Fig. 7 | Rapid cell death induced by SPI-1 ON STm is independent of cathepsin activity. Wildtype and Caspase-1/11 -/- BMDMs were infected with wildtype *S*Tm and a SPI-1 mutant (Δ*prgK*), late-exponential growing *S*Tm (SPI-1 ON) in the presence of CA-074-Me at the indicated concentrations. LDH release was measured 1.5 hpi. Boxplots are depicted as in Fig. 3C. n denotes the number of biologically independent samples.

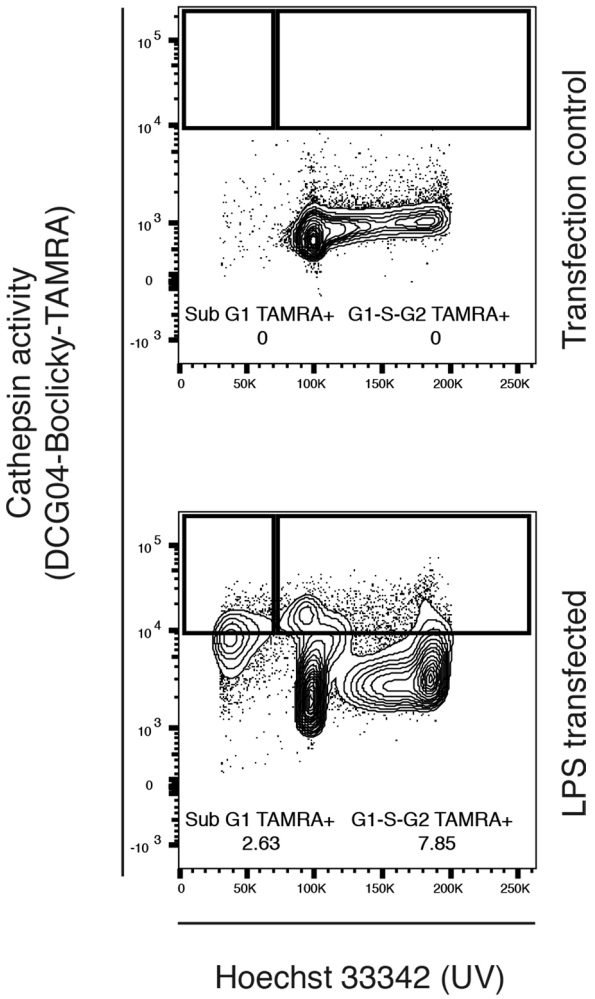

Extended Data Fig. 8 | LPS transfection promotes nuclear cathepsin activity. RAW264.7 cells were transfected with purified LPS for 20 hours. 2 hours prior to harvest cells were treated with DCG04-Boclicky-TAMRA (5 μM) to quantify nuclear cathepsin activity. Nuclei were extracted and analysed by flow cytometry as per Fig. 5A. The percentage of cathepsin positive (TAMRA+) nuclei is indicated and a second biological replicate is located in the supplementary material replicate data section.

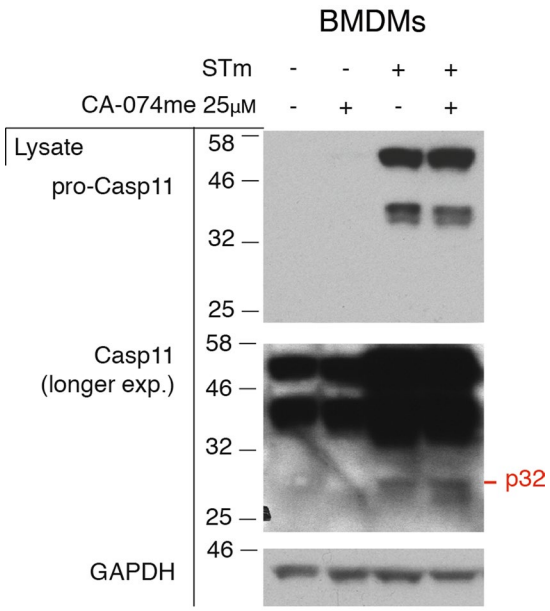

Extended Data Fig. 9 | CA-074-Me does not affect Caspase-11 expression or processing. Wildtype BMDMs were infected with wildtype *STm* for 20 hours in the presence of CA-074-Me (25 μM) or DMSO control. Lysates were probed for Caspase-11 by immunoblot and using GAPDH as a loading control. Experiment was performed once.

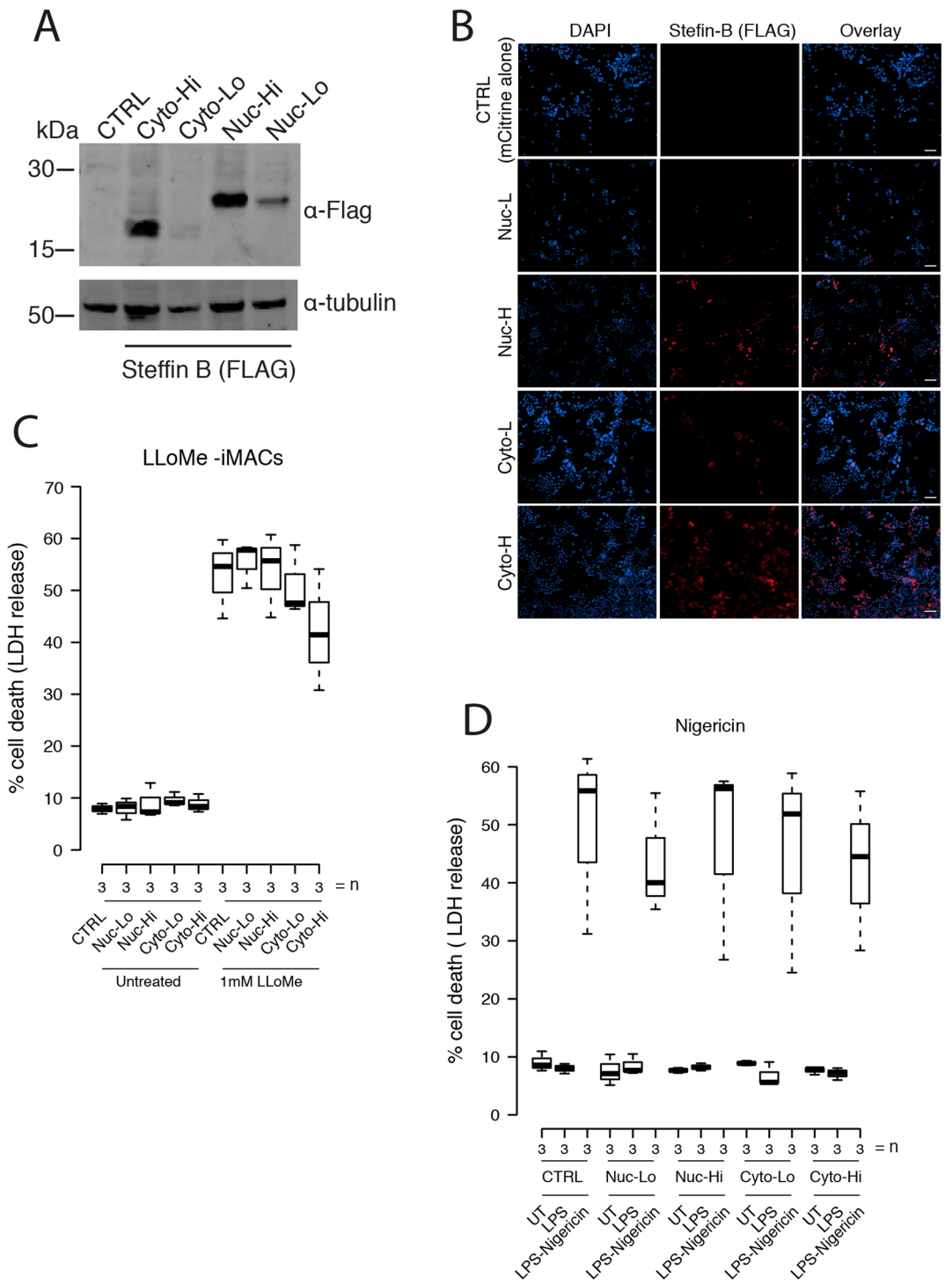

Extended Data Fig. 10 | Characterisation of iMACs expressing Stefin B targeted to the nucleus or expressed in the cytoplasm. a) Expression of Stefin B fusions targeted to either the nucleus (Nuc) or expressed in the cytoplasm (Cyto) were verified in iMAC lysates by immunoblot using anti-FLAG (M2) and anti-tubulin as a loading control. Cells were FACS sorted into high (Hi) and low (Lo) Stefin B expressing populations prior to use. Cells treated in parallel expressing mCitrine alone were used as negative controls. Experiment was repeated twice with similar results (see Supplementary Information for replicate data). b) Expression and localisation of Stefin B was assessed by microscopy in cells expressing nuclear-targeted (Nuc-Lo and Nuc-Hi) or cytoplasmic (Cyto-Lo and Cyto-Hi) Stefin B or mCitrine alone as a control. Scale bar denotes 25 μm. Experiment was repeated twice with similar results (see Supplementary Information for replicate data). c) iMACs expressing nuclear or cytoplasmic Stefin B were treated with 1 mM LLoMe or untreated and LDH release was quantified and plotted as described previously in Fig. 5b. Each data point is the combined average of biological replicate wells from three independent experiments. Boxplots are depicted as in Fig. 3c. d) iMACs expressing nuclear or cytoplasmic Stefin B were untreated, LPS treated or LPS and nigericin treated and LDH release was quantified and plotted as described previously in Fig. 5b. Each data point is the combined average of biological replicate wells from three independent experiments. Box plots are depicted as in Fig. 3c.

nature research

Corresponding author(s): Athanasios Typas

Reporting Summary

Nature Research wishes to improve the reproducibility of the work that we publish. This form provides structure for consistency and transparency in reporting. For further information on Nature Research policies, see Authors & Referees and the Editorial Policy Checklist.

Statistical parameters

When statistical analyses are reported, confirm that the following items are present in the relevant location (e.g. figure legend, table legend, main text, or Methods section).

n/a	Confirmed
☐	☒ The exact sample size (*n*) for each experimental group/condition, given as a discrete number and unit of measurement
☐	☒ An indication of whether measurements were taken from distinct samples or whether the same sample was measured repeatedly
☐	☒ The statistical test(s) used AND whether they are one- or two-sided *Only common tests should be described solely by name; describe more complex techniques in the Methods section.*
☒	☐ A description of all covariates tested
☐	☒ A description of any assumptions or corrections, such as tests of normality and adjustment for multiple comparisons
☐	☒ A full description of the statistics including central tendency (e.g. means) or other basic estimates (e.g. regression coefficient) AND variation (e.g. standard deviation) or associated estimates of uncertainty (e.g. confidence intervals)
☐	☒ For null hypothesis testing, the test statistic (e.g. *F*, *t*, *r*) with confidence intervals, effect sizes, degrees of freedom and *P* value noted *Give P values as exact values whenever suitable.*
☒	☐ For Bayesian analysis, information on the choice of priors and Markov chain Monte Carlo settings
☒	☐ For hierarchical and complex designs, identification of the appropriate level for tests and full reporting of outcomes
☐	☒ Estimates of effect sizes (e.g. Cohen's *d*, Pearson's *r*), indicating how they were calculated
☐	☒ Clearly defined error bars *State explicitly what error bars represent (e.g. SD, SE, CI)*

Our web collection on statistics for biologists may be useful.

Software and code

Policy information about availability of computer code

Data collection	Gen5 2.04 ZEN 2 (blue edition) Olympus FV31S-SW Typhoon FLA 9500
Data analysis	MaxQuant software (version 1.5.0.0) CellProfiler (v2.1.1), R (v1.0.143) FlowJo (v10.0.08) (Tree Star, Inc.) Cytoscape (v3.6.1) GraphPad Prism v(5.01) ImageJ (v2.0.0-rc-68/1.52e)

For manuscripts utilizing custom algorithms or software that are central to the research but not yet described in published literature, software must be made available to editors/reviewers upon request. We strongly encourage code deposition in a community repository (e.g. GitHub). See the Nature Research guidelines for submitting code & software for further information.

Data

Policy information about availability of data

All manuscripts must include a data availability statement. This statement should provide the following information, where applicable:

- Accession codes, unique identifiers, or web links for publicly available datasets
- A list of figures that have associated raw data
- A description of any restrictions on data availability

Proteomic data has been deposited at ProteomeXchange (http://www.proteomexchange.org/) under the identifier PXD010179 (pSILAC-AHA) and PXD016086 (2D-TPP).

Field-specific reporting

Please select the best fit for your research. If you are not sure, read the appropriate sections before making your selection.

☒ Life sciences ☐ Behavioural & social sciences ☐ Ecological, evolutionary & environmental sciences

For a reference copy of the document with all sections, see nature.com/authors/policies/ReportingSummary-flat.pdf

Life sciences study design

All studies must disclose on these points even when the disclosure is negative.

Sample size	No prior assumptions were made regarding effect sizes. SILAC experiments contained two biological replicates (reversed labels). The number of times each experiment was performed and the number of biological replicates is described in figure legends.
Data exclusions	The degree of overall batch to batch cell death displayed considerable variance. To reduce this variance, batches whereby wildtype STm induced more than >50% or <10% LDH release were removed, as described in the methods section. This aside, no data was excluded from analysis. These exclusion criteria were not pre-established.
Replication	Pearson's correlation coefficient was used to determine reproducibility between biological replicates in proteomic data. All attempts at replication were successful.
Randomization	Not relevant. All cells within a sample are clonal.
Blinding	Not relevant.

Reporting for specific materials, systems and methods

Materials & experimental systems

n/a	Involved in the study
☒	☐ Unique biological materials
☐	☒ Antibodies
☐	☒ Eukaryotic cell lines
☒	☐ Palaeontology
☐	☒ Animals and other organisms
☒	☐ Human research participants

Methods

n/a	Involved in the study
☒	☐ ChIP-seq
☐	☒ Flow cytometry
☒	☐ MRI-based neuroimaging

Antibodies

Antibodies used	anti-GAPDH-HRP(D16H11) cat. 8884. Cell Signaling. 1:1,000-1:10,000 dilution used for immunoblotting. anti-Histone H3(D1H2) cat. 4499P. Cell Signaling. 1:1,000 dilution used for immunoblotting. anti-rabbit HRP (Sigma/GE - NA934-1ML) 1:5,000 dilution used for immunoblotting. anti-mouse HRP (Sigma, HVZ-A4416-1ML). 1:5,000 dilution used for immunoblotting. anti-RNA polymerase Sigma 70 (RpoD) [2G10] Acris antibodies. cat. GTX12088. 1:1,000 dilution used for immunoblotting. anti-Caspase-11 (Novus biological 17D9, cat; NB120-10454SS). 1:5-10,000 dilution used for immunoblotting. anti-Gasdermin D (Abcam, cat; ab209845). 1:1,000 dilution used for immunoblotting. anti-Cathepsin B (R&D systems, AF965-SP). 1:2,000 dilution used for immunoblotting.

anti-Lamin A (Sigma, SAB4501764). 1:5,000 dilution used for immunoblotting.
anti-H3.cs1 was a gift from Dr. Kyung-Min Noh. 1:1,000 dilution used for immunoblotting.

Validation

anti-GAPDH-HRP(D16H11) was validated for western blot analysis according to Cell Signaling Hallmarks of antibody validation criteria.
anti-Histone H3(D1H2) cat. 4499P. was validated for western blot analysis according to Cell Signaling Hallmarks of antibody validation criteria.
anti-RNA polymerase Sigma 70 (RpoD) [2G10] Validated for western blot and immunoprecipitation.
anti-Caspase-11 (Novus biological 17D9, cat; NB120-10454SS). Validated for western blot by inducing with LPS and absence in Caspase-11 KO cells.
anti-Gasdermin D (Abcam, cat; ab209845). Verified in rodent RAW264.7 cells expressing ASC as well as GSDMD KO cells.
anti-Cathepsin B (R&D systems, AF965-SP). 1:2,000 dilution used for immunoblotting.
anti-Lamin A (Sigma, SAB4501764). 1:5,000 dilution used for immunoblotting.
anti-H3.cs1 - see relevant publication validating this antibody: Duncan, E. M. et al. Cathepsin L proteolytically processes histone H3 during mouse embryonic stem cell differentiation. Cell 135, 284–294 (2008).

Eukaryotic cell lines

Policy information about cell lines

Cell line source(s)	RAW264.7 cells (TIB71TM) were purchased at ATCC on 16.09.2014.
Authentication	ATCC authenticates its cell lines through morphology, karyotyping, and STR analyses. RAW264.7 cells were not authenticated after receipt from ATCC. Regular inspection of cell culture for coherent morphology with ATCC source images was routinely performed.
Mycoplasma contamination	Cells routinely tested negative for mycoplasma contamination.
Commonly misidentified lines (See ICLAC register)	No commonly misidentified line was used.

Animals and other organisms

Policy information about studies involving animals; ARRIVE guidelines recommended for reporting animal research

Laboratory animals	Bone marrow was collected from 8-12 week old C57Bl/6 male and female mice (Mus musculus).
Wild animals	This study did not involve wild animals.
Field-collected samples	This study did not involve samples collected from the field.

Flow Cytometry

Plots

Confirm that:

☒ The axis labels state the marker and fluorochrome used (e.g. CD4-FITC).

☒ The axis scales are clearly visible. Include numbers along axes only for bottom left plot of group (a 'group' is an analysis of identical markers).

☒ All plots are contour plots with outliers or pseudocolor plots.

☒ A numerical value for number of cells or percentage (with statistics) is provided.

Methodology

Sample preparation	Tissue culture media (DMEM 4.5 g/L glucose, 10% FBS) from RAW264.7 cells infected with Salmonella enterica Typhimurium (14028s) for 20 hours were replaced with fresh DMEM containing 5 µM DCG04-Boclicky-TAMRA, followed by a 1 hour incubation at 37°C, 5% CO2. Cells were washed thrice in PBS followed by solubilization in 0.1% Triton X-100. Nuclei were pelleted (500 xg, 3 min), washed and resuspended in PBS containing 0.1% Tx-100. Nuclei were then fixed by adding formaldehyde to 4% wt/vol (Thermo Scientific; 28908) and incubated for 15 minutes at room temperature, followed by washing in buffer containing 0.1% Triton X-100 containing 2 µg/ml Hoechst 33342. Nuclei were resuspended in 0.1% Triton X-100 containing 2 µg/ml Hoechst 33342 and subjected to flow cytometry. Nuclei samples were acquired on the Attune NxT Flow Cytometer (Thermo Fisher Scientific) equipped with 405 nm, 488 nm, 561 nm, and 638 nm lasers. Hoechst 33342 was excited by the 405 nm laser line and fluorescence signal was collected using a 440/50 bandpass filter and TAMRA excited by the 561 nm laser line and collected using a 585/15 bandpass filter. Post-acquisition analysis was done in FlowJo software 10.0.08 (Tree Star, Inc.).
Instrument	Attune NxT Flow Cytometer (Thermo Fisher Scientific)
Software	FlowJo software 10.0.08 (Tree Star, Inc.).

Cell population abundance	Flow cytometry experiments were performed on the RAW264.7 cell line and iMACs, thus the sample is a homogeneous cell population.
Gating strategy	Hoechst-stained single nuclei population was selected in a dot plot 355-450/50 width vs 355-450/50 area displayed in linear scale. The gate was placed around the target population, excluding nuclei aggregates with a higher 355-450/50 width values. Single nuclei were displayed in a dot plot 355-450/50 area vs 561-586/15 area in linear and logarithmic scale, respectively. Quadrant gates to identify TAMRA positive events were placed based on nuclei infected with STm 14028s wildtype.

☒ Tick this box to confirm that a figure exemplifying the gating strategy is provided in the Supplementary Information.